Evolutionary regain of lost gene circuit function

Mirna Kheir Gouda[a,b], Michael Manhart[c], and Gábor Balázsi[a,b,1]

[a]The Louis and Beatrice Laufer Center for Physical and Quantitative Biology, Stony Brook University, Stony Brook, NY 11794-5252; [b]Department of Biomedical Engineering, Stony Brook University, Stony Brook, NY 11794-5281; and [c]Institute of Integrative Biology, Eidgenössische Technische Hochschule Zürich, 8092 Zürich, Switzerland

Edited by James J. Collins, Massachusetts Institute of Technology, Boston, MA, and approved October 30, 2019 (received for review July 17, 2019)

Evolutionary reversibility—the ability to regain a lost function—is an important problem both in evolutionary and synthetic biology, where repairing natural or synthetic systems broken by evolutionary processes may be valuable. Here, we use a synthetic positive-feedback (PF) gene circuit integrated into haploid *Saccharomyces cerevisiae* cells to test if the population can restore lost PF function. In previous evolution experiments, mutations in a gene eliminated the fitness costs of PF activation. Since PF activation also provides drug resistance, exposing such compromised or broken mutants to both drug and inducer should create selection pressure to regain drug resistance and possibly PF function. Indeed, evolving 7 PF mutant strains in the presence of drug revealed 3 adaptation scenarios through genomic, PF-external mutations that elevate PF basal expression, possibly by affecting transcription, translation, degradation, and other fundamental cellular processes. Nonfunctional mutants gained drug resistance without ever developing high expression, while quasifunctional and dysfunctional PF mutants developed high expression nongenetically, which then diminished, although more slowly for dysfunctional mutants where revertant clones arose. These results highlight how intracellular context, such as the growth rate, can affect regulatory network dynamics and evolutionary dynamics, which has important consequences for understanding the evolution of drug resistance and developing future synthetic biology applications.

evolution | gene circuit | reversal | loss of function | bistability

Two ways for cells to survive stress and buy time until beneficial genetic alterations arise are through sensing and responding or through bet-hedging (1, 2). Gene regulatory networks evolve to provide cells with sufficient stress-protective gene expression according to these strategies. While stress-protective mutations improve the chance of survival, a tradeoff often exists between the cost and benefit of such protective mechanisms (3). For example, the expression of stress-protective genes can have a net cost in the absence of stress or even in stress if expression surpasses the levels necessary for survival (4–7). Consequently, protective but costly gene function tends to diminish or vanish from the population in the absence of stress (5, 8–10). How it might reappear again (evolutionary "reversal") when the stress resumes (11, 12) is poorly understood, specifically for gene regulatory networks that lost their costly activity. Indeed, loss-of-function mutations occur widely in laboratory evolution experiments (5, 8, 13–16), suggesting this is a common mode of adaptation to a new environment. However, few experiments have tested how such lost functions could be restored.

Besides experimental studies of natural gene-network evolution under controlled conditions (5, 8, 17–21), synthetic gene circuits can serve as well-characterized models of natural stress-response modules in evolution experiments (9, 22, 23). Well-controlled and tunable synthetic gene circuits that interact minimally with the host genome (24–27) can aid the interpretation of experimental outcomes. Considering future applications of synthetic biology (28, 29), it is important to explore potential evolutionary strategies that can restore synthetic gene circuit function if it happens to break over time (9, 30, 31), without circuit reintroduction or repair by rational means or mutagenesis (32). Directed evolution studies have improved enzymes or metabolic pathways (33, 34), but only through mutagenesis in single proteins, leaving it unclear whether noncoding or genomic mutations could improve or restore gene-network performance. Adaptation under function-restoring selection pressure allowing host genome changes could reveal essential parameters and new methods to design and improve engineered cell fitness and robustness in various growth conditions.

To understand how a network that lost its costly activity in the absence of stress adapts and possibly regains function in the presence of stress, here we used previously evolved, broken versions of a synthetic "positive feedback" (PF) gene circuit originally integrated into the haploid *Saccharomyces cerevisiae* YPH500 genome (6). Many different reverse tetracycline Transcriptional Activator (rtTA) mutants arose in previous evolution experiments (9), apparently eliminating costly rtTA function in the absence of antibiotic stress. We evolved 7 such broken PF mutants in both inducer and antibiotic, where regaining rtTA function should be beneficial. By examining the phenotypic and genetic changes through fluorescence and fitness measurements, as well as sequencing, we observed 3 different classes of evolutionary dynamics, depending on whether ancestral mutants were quasifunctional, dysfunctional, or nonfunctional. In quasifunctional mutants, slow growth from drug exposure initially enriched the high-expressor subpopulation, but then new drug-resistance mutations slightly elevated basal expression, eliminating the benefit of high expression and diminishing the high-expressor fraction through a growth-dependent shift in dynamics. Nonfunctional mutants acquired new drug-resistance

Significance

Natural or synthetic genetic modules can lose their function over long-term evolution if the function is costly. How populations can evolve to restore such broken function is poorly understood. To test the reversibility of evolutionary breakdown, we use yeast cell populations with a chromosomally integrated synthetic gene circuit. In previous evolution experiments the gene circuit lost its costly function through various mutations. By exposing such mutant populations to conditions where regaining gene circuit function would be beneficial, we find adaptation scenarios with or without repairing lost gene circuit function. These results are important for drug resistance or future synthetic biology applications where evolutionary loss and regain of function play a significant role.

Author contributions: M.K.G. and G.B. designed research; M.K.G. and G.B. performed research; M.K.G. contributed new reagents/analytic tools; M.K.G., M.M., and G.B. analyzed data; and M.K.G. and G.B. wrote the paper.

The authors declare no competing interest.

This article is a PNAS Direct Submission.

Data deposition: Data and Matlab code associated with the figures can be found at https://drive.google.com/drive/folders/13jrR8XHP4p96-bcNGTlxRpFzjTfRvPkh and https://drive.google.com/drive/folders/1sZxfXY-AzigYSCDhX_SW0bSNqfgo72lh.

[1]To whom correspondence may be addressed. Email: gabor.balazsi@stonybrook.edu.

This article contains supporting information online at https://www.pnas.org/lookup/suppl/doi:10.1073/pnas.1912257116/-/DCSupplemental.

First published November 21, 2019.

mutations that slightly elevated basal expression and never developed high expression. Finally, the dysfunctional mutant populations evolved similarly to quasifunctional mutants, but more slowly and gave rise to clones with repaired network function. Overall, we found numerous extracircuit mutations, but no novel coding-sequence mutations inside the gene circuit directly related to these expression changes. Detected genomic mutations possibly affect important cellular processes, such as transcription, translation, macromolecule degradation, and others. Our findings provide insights into the evolutionary reactivation of broken network modules, depending on their dynamics as well as the costs and benefits after the stress recurs.

Results

Hyperinduction and Slow Growth Reveal 3 Classes of rtTA Mutations. The original PF gene circuit (6) consists of a doxycycline (Dox)-inducible rtTA transcriptional activator that identically upregulates both its own expression and the expression of the Zeocin resistance gene, *zeoR*, fused to yEGFP (*yEGFP::zeoR*), by binding to 2 *tetO2* operator sites upstream of the *rtTA* and the *yEGFP::zeoR* coding regions (Fig. 1*A*). The yEGFP::ZeoR bifunctional fusion protein (35) precisely reports ZeoR levels and protects cells by directly binding to Zeocin (36) to prevent its intercalation into DNA, which causes DNA breaks and thus cell cycle arrest or death (37). Previously, we evolved yeast populations carrying the PF circuit (9) in 2 μg/mL of Dox inducer without Zeocin antibiotic, a condition denoted "D2Z0," where the first number represents Dox concentration in micrograms per milliliter, while the second number represents Zeocin concentration in milligrams per milliliter. Since the activation of the PF stress-response module is costly in the absence of stress, the rtTA protein apparently lost its function during these evolution experiments through different coding-sequence mutations (9). To test whether evolutionary repair of lost rtTA function was possible, we further evolved 7 of these loss-of-function rtTA mutants from the previous experiment (Fig. 1*B*) in the condition D2Z2 (2 μg/mL Dox and 2 mg/mL Zeocin), which should activate the original PF gene circuit or any reverting mutants, ensuring their survival in stress. We will refer to the 7 ancestral mutations by their genotype: "Missense 1, 2, 3, and 4" correspond to $rtTA_{+189C\rightarrow G}$, $rtTA_{+562T\rightarrow C}$, $rtTA_{+275G\rightarrow A}$, and $rtTA_{+13G\rightarrow T}$, respectively; "Nonsense" corresponds to $rtTA_{+442G\rightarrow T}$; "Duplication" corresponds to $rtTA_{+95,\ 30bp}$; and "Deletion" corresponds to $rtTA_{+651,\ 78bp\Delta}$ (*SI Appendix*, Table S1).

To understand the dynamics of the original PF gene circuit (Fig. 1*A*) and its 7 rtTA mutants (Fig. 1*B*), we studied qualitatively a simple mathematical model of this genetic autoregulatory module (*SI Appendix*, *Mathematical Modeling*). In rate-balance plots from these models (Fig. 1*C*), intersections between rtTA synthesis (Fig. 1*C*, blue sigmoid) and loss (Fig. 1*C*, red elbow) rate curves correspond to stable (Fig. 1*C*, full circles) and unstable (Fig. 1*C*, open circles) *rtTA* gene expression states that impose corresponding cellular yEGFP::zeoR protein levels. For example, the original PF gene circuit (6) is monostable below a threshold

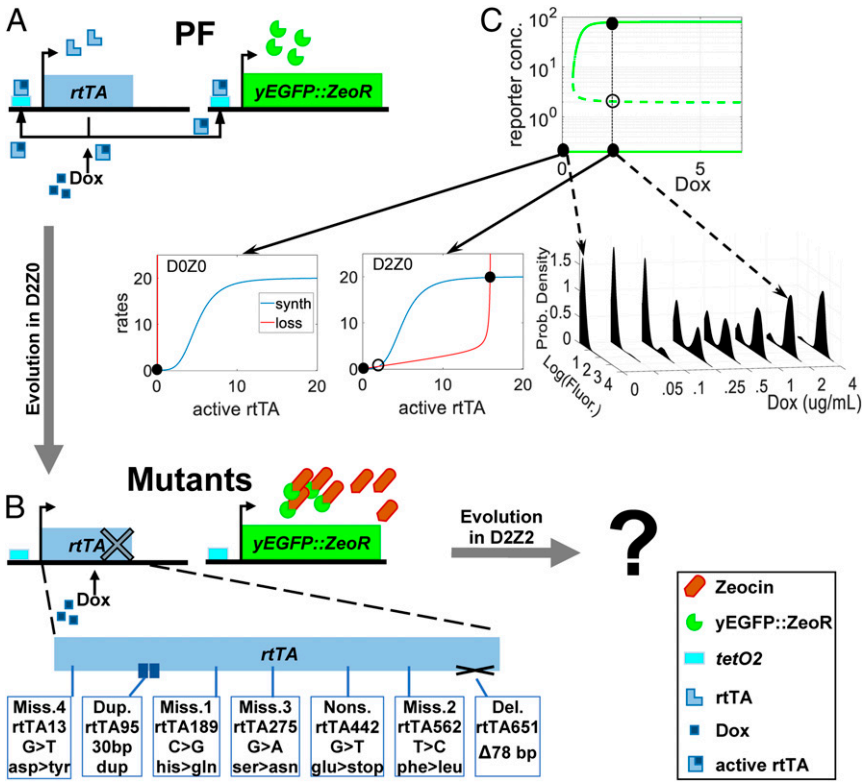

Fig. 1. The PF gene circuit lost bistability and costly rtTA function by multiple mutations. (*A*) In the original PF gene circuit, the inducer Dox binds and activates the rtTA protein, which identically activates its own *rtTA* gene and *yEGFP::zeoR*. Since rtTA activity is costly, loss of rtTA function is evolutionarily beneficial in D2Z0. (*B*) We selected 7 mutants that arose in D2Z0, each improving fitness by PF breakdown. Now we evolve each mutant in D2Z2 where regaining rtTA function would be beneficial. DxZy denotes the concentrations of the inducer Dox and the antibiotic Zeocin in micrograms per milliliter and milligrams per milliliter, respectively. (*C*) The original PF gene circuit undergoes a saddle-node bifurcation, changing from monostable to bistable dynamics when Dox exceeds a threshold. The top graph shows yEGFP::zeoR levels versus Dox from a simple mathematical model (*SI Appendix*, *Mathematical Modeling*). The blue and red curves on the bottom graphs represent inactive rtTA synthesis and loss rates; while filled and open circles denote stable and unstable steady states, respectively. The active rtTA levels corresponding to the circles impose the yEGFP::zeoR levels on the top graph and on the right, where experimental yEGFP::zeoR expression histograms versus Dox demonstrate the bifurcation.

concentration of ~0.05 μg/mL Dox, with a single intersection corresponding to a single low rtTA expression state imposing low yEGFP::zeoR expression. As Dox concentrations increase, the elbow-shaped curve of Dox-free, inactive rtTA loss (from combined dilution and degradation) moves rightward, approaching the sigmoidal rtTA synthesis curve until they meet and intersect 3 times. Thus, for Dox concentrations above the threshold, a second stable high-expression state emerges, indicating a transition from monostable to bistable dynamics through a saddle-node bifurcation (Fig. 1*C*). Losing the high gene-expression peak during long-term evolution in D2Z0 (9) could indicate either that a mutant gene circuit became completely noninducible, or that the sigmoidal rtTA synthesis rate curve shifted somehow, elevating the bistability threshold beyond D2Z0. Still, the elbow-shaped loss curve slides rightward as Dox increases further, so it could still reach and intersect a right-shifted sigmoid curve 3 times, causing a high-expression peak to still emerge at sufficiently high Dox concentrations. To examine the possibility of such weaker but still present rtTA function, we looked for high expressors in flow cytometry histograms of each mutant in D2Z0. Indeed, upon closer examination, we noticed ~1% high-expressing cells in Missense 1 and 2 populations, but not any other mutants (*SI Appendix*, Figs. S3–S8). Therefore, we deem the Missense 1 and 2 mutant gene circuits to be quasifunctional rather than completely nonfunctional (*SI Appendix*, Table S1).

To fully test which of the 7 loss-of-function PF mutants are still quasifunctional, we next hyperinduced them with excess Dox. We expected that hyperinduction would shift the elbow-shaped curve of rtTA loss farther rightward and move quasifunctional rtTA mutants into their bistable regime (Fig. 1*C* and *SI Appendix*, *Mathematical Modeling*), thus generating high-expressor subpopulations, while nonfunctional mutants would remain unimodal. To this end we grew clonal populations carrying each rtTA mutation in D6Z0 (Fig. 2 *A* and *B*), a 3-fold higher (6 μg/mL) Dox concentration than D2Z0 where they previously arose. These hyperinducing conditions confirmed that Missense 1 and 2 were indeed quasifunctional, while the remaining 5 mutants—Missense 3 and 4, Nonsense, Duplication, and Deletion—still appeared uninducible and thus nonfunctional (*SI Appendix*, Table S1). Excess Dox did not alter the growth rate of any clones, indicating that hyperinduction is not toxic for any mutant. Thus, any further mutations abolishing leftover rtTA function in Missense 1 and 2 would not be beneficial. The results did not change upon hyperinducing the mutants in 8 μg/mL Dox (*SI Appendix*, Fig. S1*A*). Hysteresis experiments also confirmed the upshift of bistability range for Missense 1 and 2 compared to PF (*SI Appendix*, Fig. S2).

Mathematical models suggested another mechanism besides hyperinduction that can cause stable high expression. Slow growth reduces dilution of cell contents and thus tilts downward the rtTA loss curve, besides shifting it rightward. This moves the quasifunctional PF mutants into the bistable regime (*SI Appendix*, *Mathematical Modeling*), similar to growth-mediated bistability observed in other systems (38, 39). To experimentally test this, we grew PF mutants as well as standard PF cells in D2Z0 with 7.5% ethanol that slowed the growth rate to a value similar to that in D2Z2 (*SI Appendix*, Figs. S3–S8). Interestingly, ethanol strongly enriched the high-expressor fraction of ancestral PF cells, from 71 to 91% in D2Z0. As expected, slow growth due to ethanol also enriched the high-expressor fractions of Missense 1 (more than 2-fold) and Missense 2 (about 9-fold). Most surprisingly, ethanol caused a few high-expressor cells to appear even in Missense 3, which failed to respond to hyperinduction in D6Z0 or D8Z0. Therefore, we classify Missense 3 as a dysfunctional mutant (*SI Appendix*, Table S1), unlike the nonfunctional mutants Nonsense and Deletion, which do not become bistable even in slow growth. We obtained comparable results using Cisplatin, which interferes with DNA (40) like Zeocin (37). In contrast, G418 did not have this effect,

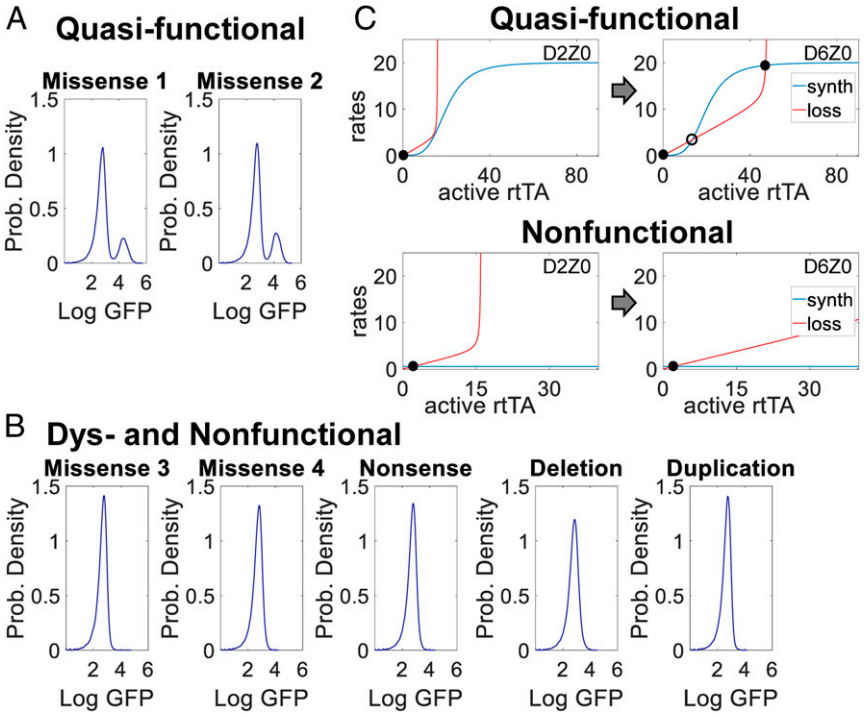

Fig. 2. Quasifunctional rtTA mutants revealed by hyperinduction. (*A* and *B*) Gene-expression histograms of quasifunctional, dysfunctional, and nonfunctional PF mutants hyperinduced in D6Z0 (24 h). A high-expression peak in this condition indicates bistabiltiy. (*C*) Plots illustrating the dynamical effect of hyperinduction on quasifunctional and nonfunctional PF mutants. Filled and open circles denote stable and unstable steady states, respectively.

presumably because protein synthesis inhibition (41) abolishes gene circuit function (*SI Appendix*, Figs. S3–S8). Overall, these data and the model indicate that slow growth due to stressors can cause shifts in dynamics that generate high expressors in Missense 3 and can enrich the already present high expressor subpopulations of Missense 1 and 2.

Evolution Does Not Revert Quasifunctional Mutants. Next, we set out to test if evolution could revert the 2 quasifunctional mutants (Missense 1 and 2) to regain stronger rtTA function. Thus, we evolved 3 replicates each of Missense 1 and 2 in D2Z2 medium, where regaining high rtTA activity would beneficially shift cells into the drug-resistant state of high yEGFP::ZeoR expression. For control purposes, we also propagated the same initial populations in D2Z0.

We observed qualitatively similar evolutionary dynamics for both Missense 1 and 2 (Fig. 3), which started with a minimal (0.47% and 0.63%) subpopulation of high-expressor cells immediately upon transfer from D2Z0 into D2Z2. Early on, population fitness levels dropped significantly in all D2Z2 cultures compared to the control D2Z0 cultures (Fig. 3 *C* and *D*). Soon afterward, drug exposure generated a substantial high-expressing subpopulation for a few days (Fig. 3 *A* and *B*). Growth rates started recovering in ∼4 d, as the high-expressor peak increased (Fig. 3 *C* and *D*). From day 1 onward, we also observed a slight upward fluorescence shift for low expressors, corresponding to elevated basal yEGFP::ZeoR levels compared to D2Z0 controls (Fig. 3 *A* and *B*). This slight upward expression shift is clearly distinguishable from "induced" high expression and resembles phenotypes arisen previously during evolution in Zeocin drug (D0Z2) (9), where various extracircuit mutations, often coupled with intracircuit synonymous and promoter mutations, elevated the low, basal yEGFP::ZeoR expression. Concurrently, the high-expressor population fraction reached a maximum around day 4 and then returned to the same low level as in D2Z0 within ∼8 d (Fig. 3 *A* and *B*).

Considering that high expressors were rare in D2Z0, while in D2Z2 their fraction initially increased and then later dropped back to the D2Z0 level, at least 2 hypotheses are possible. First, compensatory mutations in rtTA or elsewhere could improve rtTA activator function, thereby increasing the high-expressor fraction, and then later subsequent mutations could revert this effect. To identify such compensatory mutations, we performed whole-genome sequencing (WGS) on 1 replicate population each for both mutants on days 1, 3, and 14. The original rtTA mutations already present at the beginning of the experiment were identified at 100% frequency at all time points for both Missense 1 and 2. However, we identified no other intracircuit mutations. Since certain variant types (e.g., deletions and duplications) in the PF gene circuit are difficult to detect by WGS (24), we also performed Sanger sequencing of the PF region in 10 individual clones from each mutant at day 14 (*SI Appendix*, Table S2). All Missense 1 clones carried a deletion of the first *tetO2* operator upstream of the *yEGFP::zeoR* coding region, whereas the other *tetO2* site stayed intact. All Missense 2 clones carried only their original gene circuit mutation without any *tetO2* or other circuit modifications, despite their identical phenotypes to Missense 1. Therefore, there is no phenotypic signature directly and specifically attributable to the *tetO2* operator site deletion (*SI Appendix*, Table S3). Overall, the only de novo intracircuit mutation we found did not explain the observed gene-expression changes.

High expression requires rtTA function. How then could a substantial high-expressor peak emerge and later diminish without any changes in the rtTA coding sequence or its promoter? Modeling and experiments suggested a second hypothesis: By

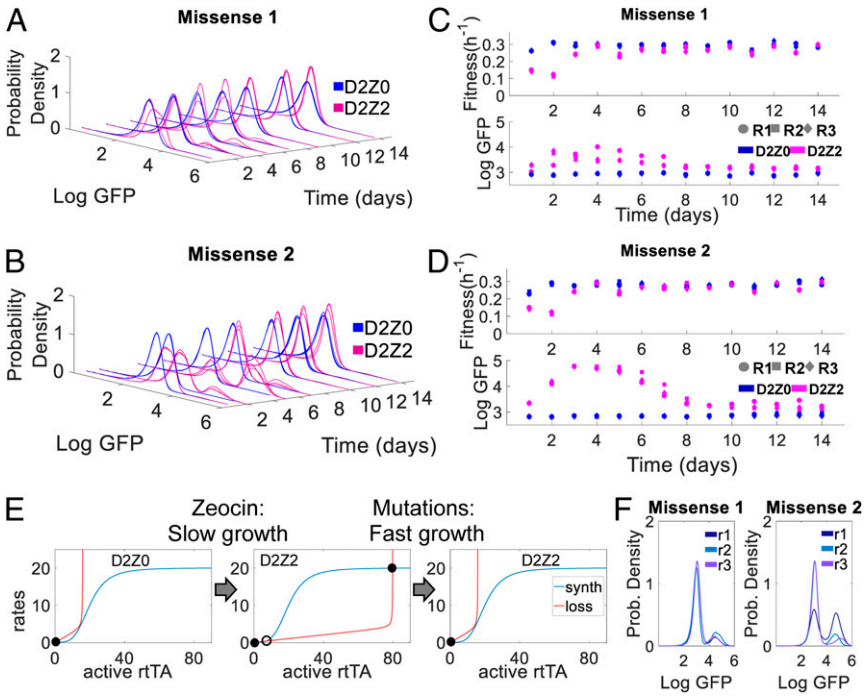

Fig. 3. Evolutionary dynamics of quasifunctional mutants. (*A* and *B*) Histogram of *yEGFP::zeoR* expression for Missense 1 and 2 replicates in D2Z0 (blue, control) and D2Z2 (magenta) over the course of 14 d. (*C* and *D*) Population fitness of Missense 1 and 2 replicates in D2Z0 (blue) and D2Z2 (magenta) over the course of 14 d. (*E*) Changes of PF dynamics due to slower growth and selection in Zeocin, and then, reversion to normal growth in D2Z2 after the emergence of drug-resistance mutations. Filled and open circles denote stable and unstable steady states, respectively. (*F*) Gene-expression histograms of evolved Missense 1 and 2 population replicates hyperinduced in D6Z0 at the end of experimental evolution. A high-expression peak in this condition indicates the presence of quasifunctional mutants in the population.

decelerating growth and reducing dilution, Zeocin tilts downward and shifts rightward the red elbow curve of rtTA loss (Fig. 3*E*). This causes a shift in dynamics (*SI Appendix*, *Mathematical Modeling*) that enriches the rare high-expressing drug-resistant cells that preexist in D2Z0 (*SI Appendix*, Figs. S3 and S4), which are then further enriched by phenotypic selection. At the same time, the low-expressing subpopulation will remain drug-sensitive, enabling any mutants that elevate basal expression to grow faster and spread in the population. Once such fast-growing mutants arise, their faster growth/dilution rate tilts upward and shifts leftward the red elbow curve (Fig. 3*E*), causing a return of dynamics toward monostability (*SI Appendix*, *Mathematical Modeling*). Concurrently, the benefits of high-expression also vanish, causing the high-expressor fraction to diminish back to the D2Z0 levels. Importantly, these events can occur without any mutations in the PF gene circuit, as long as extracircuit mutations can raise basal yEGFP::ZeoR expression to promote fast growth in Zeocin.

To identify such extracircuit mechanisms of *yEGFP::zeoR*-dependent Zeocin resistance, we looked for genomic, extracircuit mutations in the WGS data (*Materials and Methods*). In the Missense 1 population at day 14 we found moderate-frequency (~15%), nonsynonymous mutations in 2 genes affecting protein stability and transcription, *PAH1* and *SET3*, including a 1-bp frameshift deletion in the latter. Additional mutations in other genes and intergenic regions exist at lower frequencies (SI Appendix Table S3 and Dataset S1). In contrast to Missense 1, evolved Missense 2 populations carried multiple extracircuit mutations exceeding 90% in frequency at day 14 (*SI Appendix*, Table S3 and Dataset S2). Mutations in the genes *PHB2*, *MDM32*, and *COX1* suggest alteration in mitochondrial metabolism and function. We also observed a synonymous mutation in the FG-nucleoporin *NUP159* gene, which is involved in posttranscriptional regulation (42).

To test if elevated *yEGFP::zeoR* gene expression mediates drug resistance without rtTA activity, we compared the growth of Missense 1- and 2-evolved populations and clonal isolates to their unevolved Missense 1 and 2 ancestors in Zeocin-only media (D0Z2). Evolved Missense 1 and 2 populations and clonal isolates grew significantly faster than the ancestral PF or unevolved Missense 1 and 2 cells in D0Z2 (*SI Appendix*, Figs. S12 and S13), indicating that the evolved Missense 1 and 2 populations were Zeocin-resistant independently of rtTA.

If the *rtTA* coding sequence and PF gene circuit dynamics did not change during evolution, hyperinduction should affect Missense 1 and 2 similarly to their ancestors. To test this, we hyperinduced each final evolved Missense 1 and 2 replicate population in D6Z0. Indeed, the evolved Missense 1 and 2 populations developed high expression in D6Z0 (Fig. 3*F*) and in D8Z0 (*SI Appendix*, Fig. S1*B*) as their ancestors did. Similarly, hyperinduction did not affect the growth rates of the evolved populations. Overall, the Missense 1 and 2 evolution experiments indicate that slow growth and phenotypic selection initially enrich the high-expressor fraction nongenetically, but then extracircuit mutations accelerate growth by elevating basal stress-protective yEGFP::ZeoR expression, which shifts the dynamics to diminish the high-expressor fractions back to levels equivalent to D2Z0.

Most Nonfunctional Mutants Never Regain rtTA Function. As the lack of high expression in D6Z0 indicates, the 4 other initial PF mutants (Missense 4, Nonsense, Duplication, and Deletion) had mutations that disrupted rtTA protein function such that it became completely uninducible, regardless of inducer amount (Fig. 2*B* and *SI Appendix*, Fig. S1*A*) or growth rate (*SI Appendix*, Figs. S6 and S7). To test if evolution could restore rtTA function in any of these nonfunctional mutants, we also evolved 3 replicates of each in D2Z2 where regaining rtTA activity would generate a beneficial high *yEGFP::ZeoR* expression peak.

Early in the evolution experiment (Fig. 4*B* and *SI Appendix*, Fig. S9 *A–F*), the growth rate in D2Z2 of each nonfunctional mutant population dropped significantly below the controls evolving in D2Z0. The growth rates of the Missense 4, Nonsense, and Duplication populations then recovered over ~5 d, while the growth rates of the Deletion populations recovered within 3 d, approaching that of D2Z0 control cultures. Unlike quasifunctional mutants, nonfunctional mutants never gave rise to a high-expressor subpopulation (Fig. 4*A* and *SI Appendix*, Fig. S9 *A–C*). The *yEGFP::zeoR* expression distributions remained unimodal but shifted slightly upwards compared to the basal (D2Z0 control) expression in all experimental cultures. Consequently, these evolving cell populations relied again on *yEGFP::zeoR* expression to gain drug resistance and increase their fitness, without repairing rtTA function. Indeed, Sanger sequencing of 10 isolated clones from each mutant revealed no additional mutations inside the gene circuit, except for the deletion of the first *tetO2* site upstream of *yEGFP::zeoR* in 0 of 10 Missense 4 clones, 1 of 10 Nonsense clones, 8 of 10 Deletion clones, and 2 of 10 Duplication clones (*SI Appendix*, Table S4). All mutants retained the original rtTA mutation and no other rtTA mutations were detected. As with Missense 1 and 2, there was no phenotype associated specifically with the *tetO2* deletion (*SI Appendix*, Table S4).

To identify possible extracircuit mutations causing the slight basal expression increase, we analyzed the WGS data. We found mutations in or near genes controlling mRNA and protein levels through degradation or synthesis, such as the poly-A tail shortening *CCR4*, the TFIID subunit *TAF2*, the ribosomal subunit *RPL41A*, and others (Datasets S4–S7).

To examine rtTA nonfunctionality at the end of the evolution experiment, we hyperinduced final evolved populations in D6Z0. As expected, the yEGFP::ZeoR expression of nonfunctional mutants remained unimodal and low in D6Z0 and in D8Z0 (Fig. 4*C* and *SI Appendix*, Figs. S1*B* and S9*G*), indicating that rtTA and the gene circuit in these mutants remained nonfunctional at the end of evolution in D2Z2, as anticipated.

As we did for Missense 1 and 2, we also examined rtTA-independent Zeocin resistance of nonfunctional mutants by growing evolved populations and isolated clones in D0Z2 media

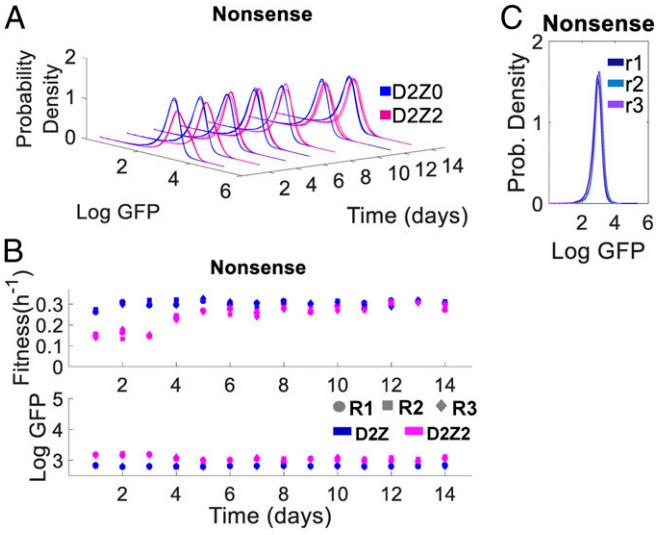

Fig. 4. Example of evolutionary dynamics of nonfunctional mutants that never regain rtTA function. (*A*) Histograms of *yEGFP::zeoR* expression of 3 replicates of Nonsense mutant in D2Z0 (blue, control) and D2Z2 (magenta) over the course of 14 d. (*B*) Fitness and mean *yEGFP::zeoR* expression plots for Nonsense mutant computed for each day of the experiment. (*C*) Gene-expression histograms of evolved population replicates hyperinduced in D6Z0 at the end of experimental evolution.

for 24 h. The evolved Missense 4, Nonsense, and Duplication populations and isolated clones grew significantly faster than their unevolved ancestors (*SI Appendix*, Figs. S12 and S13). Interestingly, the unevolved Deletion mutant seemed to have some preexisting yEGFP::ZeoR-dependent resistance to Zeocin (*SI Appendix*, Figs. S12 and S13). This corroborates the faster Deletion recovery and slightly higher yEGFP::ZeoR basal expression compared to all other nonfunctional mutants upon Zeocin exposure, already at day 1 (*SI Appendix*, Fig. S10), and reinforces general reliance on slightly elevated yEGFP::ZeoR expression for drug resistance.

Dysfunctional Mutants Can Regain PF Gene Circuit Function. Surprisingly, during evolution in D2Z2, all 3 replicates of the dysfunctional rtTA mutant (Missense 3) temporarily gave rise to a significant high-expressor subpopulation that persisted for over a week for each replicate. Ultimately, toward the end of the evolution experiment, these high-expressor subpopulations diminished and the fluorescence shift of the low peak indicated a slight increase in basal yEGFP::zeoR expression similar to all other genotypes. The fitness trends of each Missense 3 replicate resembled those of the other mutants: The initially low population fitness levels recovered to normal (control) levels within ~4 d (Fig. 5 *A* and *B*).

Once again, despite the marked appearance and subsequent gradual disappearance of the high-expressing peak in D2Z2, we found no additional rtTA coding sequence mutations in Missense 3 populations. Sanger sequencing from day 14 detected only 1 intracircuit mutation in some clones: The deletion of 1 *tetO2* site upstream from yEGFP::zeoR, while the other *tetO2* sites remained intact. Interestingly, all individual Missense 3 clones that acquired a *tetO2* deletion had unimodal gene expression, whereas the clones that lacked this mutation were bistable in D2Z2 at the end (*SI Appendix*, Table S5).

Mathematical modeling (*SI Appendix*, *Mathematical Modeling*) suggested that gene circuit dysfunction in Missense 3 is due to a drop in rtTA activator capacity (Fig. 5*C*), rather than reduced inducer sensitivity as for Missense 1 and 2. This means that the rtTA synthesis rate curve collapses downward (Fig. 5*C*) instead of shifting rightward (Fig. 2*C*) in such dysfunctional mutants. Importantly, this collapse implies that the elbow-shaped rtTA loss curve will always be above the collapsed sigmoid during normal growth, so the curves will miss intersecting each other again regardless of the hyperinducing Dox level. Yet, a bistable region can still be reached if slow growth/dilution tilts downward and shifts rightward the rtTA loss curve, causing high-expressors to emerge, despite Missense 3 being completely unresponsive to hyperinduction. Indeed, adding ethanol or Cisplatin but not G418 to D2Z0 indicated that slow growth enables some high expression in Missense 3 (*SI Appendix*, Fig. S5). Zeocin in D2Z2 enriches this high-expressor fraction further by selection. Mutations elevating the entire sigmoidal synthesis curve could then accelerate growth, thus reestablishing and maintaining bistability (Fig. 5*C*), while also stabilizing the high-expressor fraction (*SI Appendix*, *Mathematial Modeling*). On the other hand, not all mutations elevate expression sufficiently to maintain bistability as growth accelerates, causing the high-expressor fraction to diminish in the evolving population, which can be a mixture of such mutation types.

To identify these mutations predicted by the model, we examined WGS data for 2 replicate populations of Missense 3. Relevant high-frequency mutations potentially related to transcriptional regulation in replicate 1 (r1) included 1-bp frameshift deletions in *SIF2* and *SSN3*, as well as a nonsynonymous mutation in *SSN2*. Missense 3 replicate 3 (r3), on the other hand, carried multiple genomic mutations that spread in the entire population by day 14 of the experimental evolution, including missense mutations in mediator complex components *SRB8* and *MED6*, both of which are involved in RNA polymerase II-dependent transcriptional regulation (43–45) and could elevate both basal and maximal rtTA levels (the entire rtTA synthesis curve) as the model suggested. In addition, a chaperonin subunit *CCT7* mutation suggests effects on general protein folding (46), and mutations in the *SAP185* and *EXG1* coding regions suggest altered cell cycle regulation (47, 48) (*SI Appendix*, Table S5 and Dataset S3).

We also hyperinduced the final evolved replicate populations from Missense 3 in D6Z0 to examine PF function at the end of evolution. Surprisingly, 2 evolved Missense 3 replicates (r1 and r3) had bimodal distributions, indicating that gene circuits in some clones became quasifunctional or fully functional.

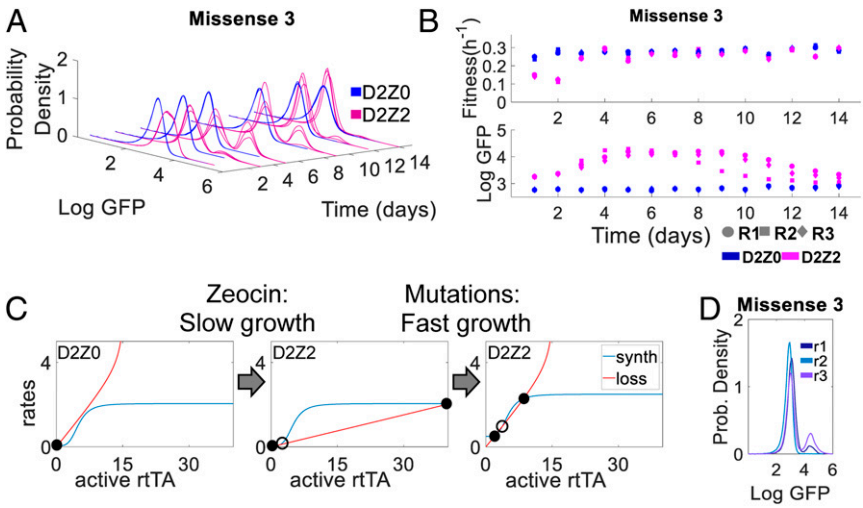

Fig. 5. Evolutionary dynamics of the dysfunctional mutant Missense 3. (*A*) Histogram of *yEGFP::zeoR* expression of Missense 3 replicates in D2Z0 (blue, control) and D2Z2 (magenta) over the course of 14 d. (*B*) Population fitness mean *yEGFP::zeoR* of Missense 3 cells in D2Z0 (blue) and D2Z2 (magenta) over the course of 14 d. (*C*) Evolutionary changes in gene circuit dynamics involve slow growth-induced bistability due to Zeocin, followed by extracircuit mutations that can shift the entire rtTA synthesis curve upward, reestablishing bistability. Filled and open circles denote stable and unstable steady states, respectively. (*D*) Gene-expression histograms of evolved population replicates hyperinduced in D6Z0 at the end of experimental evolution. A high-expression peak in this condition indicates the presence of quasi- or fully functional revertant mutants in the population.

Missense r2 had a unimodal distribution in D6Z0, indicating that it remained insensitive to hyperinduction (Fig. 5*D*). We observed the same in D8Z0 (*SI Appendix*, Fig. S1*B*).

Finally, as for other mutants, we assessed rtTA-dependence of Zeocin resistance in evolved Missense 3 populations and clonal isolates by culturing them in D0Z2. OD600 measurements of original and evolved populations (*SI Appendix*, Figs. S12 and S13) indicated that evolved Missense 3 replicate populations grew significantly faster than their unevolved ancestor. Interestingly, isolated bimodal Missense 3 clones with mutation-free gene circuits grew slower in D0Z2 than unimodal clones with a *tetO2* site deletion upstream from *yEGFP::zeoR*. This further supports that the *tetO2* site deletion contributes to *rtTA*-independent, but *yEGFP::zeoR*-dependent drug resistance, whereas bimodal Missense 3 clones rely on regained rtTA activity for resistance.

Sorting Dysfunctional Mutants Yields Clones with Regained rtTA Function. So far, a likely common explanation for the observed evolutionary dynamics is the appearance and spread of extra-circuit mutations that accelerate growth of the drug-sensitive, low-expressor subpopulation by elevating *yEGFP::zeoR* basal expression, thereby returning the dynamics toward the unimodal low-expression regime. If this is the case, then separating the high- and low expressors around day 4 should result in different evolutionary dynamics. Since drug selects against ancestral low-expressor cells, the increased selection pressure should cause drug-resistance mutations to spread quickly among low-sorted cells, preventing them from generating a substantial high-expressing peak. On the other hand, high-sorted cells would be insensitive to Zeocin and mutations could spread among them only after they generate a low-expressing peak by phenotypic switching. Therefore, high-sorted cells should take longer to become unimodal than low-sorted cells. Also, as discussed above, some quasi- or fully functional PF revertant clones may exist. If any revertant strains arose, we may be able to isolate them among the high-sorted cells because high expression is the hallmark of PF functionality.

To test these hypotheses, we separated the low-expressor and high-expressor subpopulations by fluorescence-activated cell sorting (FACS) at the end of day 4 of the original evolution experiment and cultured these high- and low-sorted subpopulations separately in the D2Z2 condition for 12 d (Fig. 6). As predicted, Missense 1 and 2 low-sorted subpopulations remained in the low-expression state throughout this experiment, indicating rapid takeover by genomic mutations conferring drug resistance. Accordingly, the corresponding high-sorted subpopulations generated bimodal distributions that became unimodal only after a few days as expected.

As opposed to Missense 1 and 2, Missense 3 low-sorted subpopulations transiently gave rise to new high-expressor subpopulations (Fig. 6 *A*–*C*), indicating either that basal expression-elevating mutants spread much more slowly than in Missense 1 and 2, or that revertant strains arose. For low-sorted Missense 3 replicates r2 and r3, the high-expressor peak gradually diminished within ∼9 d. In contrast, low-sorted Missense 3 r1 remained stably bimodal from day 5 throughout the end of this 12-d postsort experiment (Fig. 6 *C* and *F*).

High-sorted subpopulations from all 3 Missense 3 replicates gave rise to low-expressor cells within 1 d after flow sorting. Eventually, the high-expressor peak diminished in all high-sorted subpopulations, except as above, for Missense 3 r1, which

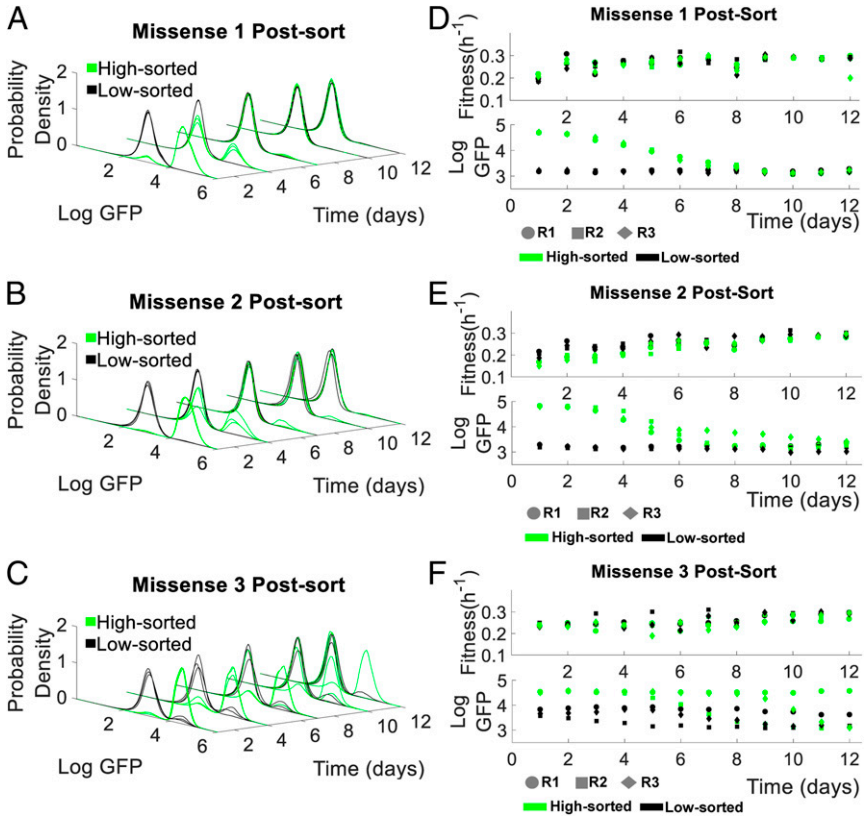

Fig. 6. Postsort evolutionary dynamics of low-sorted and high-sorted subpopulations. (*A*–*C*) Histograms of *yEGFP::zeoR* expression for Missense 1, Missense 2, and Missense 3 low-sorted (black) and high-expressor (green) subpopulations. (*D*–*F*) Population fitness and mean *yEGFP::zeoR* expression of Missense 1, Missense 2, and Missense 3 low-sorted (black) and high-sorted (green) subpopulations over the course of 12 d.

remained stably bimodal, biased toward the high-expression state for the last 7 d postsort (Fig. 6 *A*–*C*). Therefore, some Missense 3 r1 clones must be revertant strains with stable high expression.

To identify PF circuit genetic changes underlying these phenotypes, we Sanger-sequenced the *yEGFP::zeoR* and *rtTA* regions of 5 such individual revertant clones. Once again, the PF sequence in revertant clones was genetically identical to the original Missense 3 mutant. WGS (Dataset S3) revealed 1 mutation in the *SSN2* gene that spread in the high-sorted Missense 3 r1 population over time (reaching 62.2% on day 12 postsort), suggesting that it confers a survival benefit and is associated with the stable high-expression peak in this population. This mutation was also present at lower frequencies (5.6% and 6.6%) in the respective unsorted and low-sorted populations, further supporting its association with functional reversion. The *SSN2* gene encodes an RNA polymerase II mediator complex subunit essential for transcriptional regulation, resembling the general transcriptional-regulatory function of mutations in Missense 2 and 3 r3 (*SI Appendix*, Tables S3 and S5). However, the dynamic consequences of such gene-expression increases depend on the original mutation (i.e., whether it shrinks or right-shifts the sigmoidal rtTA-synthesis function).

If fully functional revertant strains arose from Missense 3, they should be clearly bimodal in D2Z0, without Zeocin. Thus, to further characterize revertant strains, we studied the yEGFP::zeoR fluorescence distribution in 5 individual Missense 3 r1 clones at the end of the postsort experiment (on day 12) in D2Z2, D0Z2, D2Z0, and D0Z0 for 4 d. Based on these experiments, Missense 3 r1 revertant clones fell into 2 phenotypic categories: Some had approximately equal peak heights in D2Z2 and D2Z0, whereas other clonal populations consisted almost exclusively of high expressors (Fig. 7 *A* and *B* and *SI Appendix*, Fig. S11) like the ancestral PF. Remarkably, the mutations conferred stable high expression even without Zeocin. Additionally, maximum expression shifted leftward, causing the peaks to approach each other compared to the ancestral PF, as predicted by sigmoid elevation in the *SI Appendix* model (*SI Appendix*, *Mathematical Modeling*). Remarkably, the distributions were very similar in D2Z2 and D2Z0, indicating that the revertant strains were drug resistant at all expression levels (*SI Appendix*, Fig. S14), so Zeocin did not select for high expression.

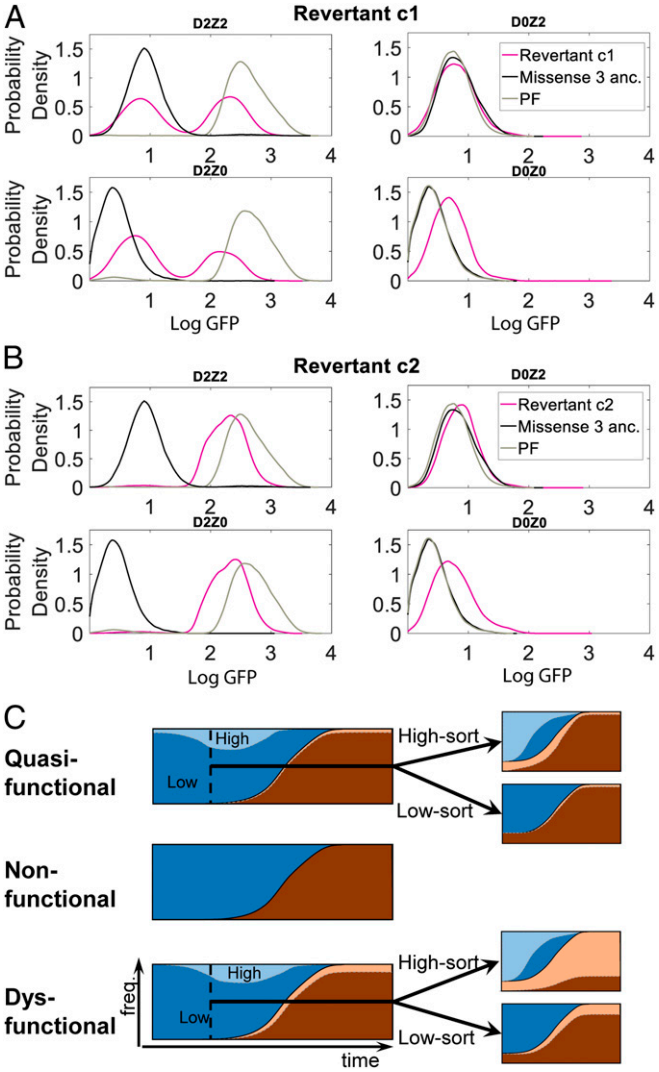

Fig. 7. Phenotypic characterization of revertant clones. (*A*) Clone 1 from day 12 of high-sorted Missense 3 r1 populations is a representative of revertant clones with approximately equal gene-expression peaks in D2Z2 and D2Z0. (*B*) Clone 2 from day 12 of high-sorted Missense 3 r1 populations is a representative of Missense 3 clones with predominantly high expressors. Histograms were recorded after maintaining each population over 4 d in each indicated condition. (*C*) Muller plot cartoons illustrating schematically time-dependent phenotypic and genotypic frequencies (evolutionary dynamics) during pre- and postsort experimental evolution for quasifunctional, nonfunctional, and dysfunctional PF mutants. Different colors indicate different genotypes. Different shades of the same color indicate different phenotypes associated with the same genotype in bistable populations, the lighter shade corresponding to high expression. The plots ignore phenotypically equivalent competing genotypes for simplicity. For the dysfunctional mutant Missense 3 the plots illustrate only the revertant clone.

Discussion

Loss-of-function is widely observed in experimental evolution studies (5, 8, 13–16), presumably because of the large supply of mutations having these effects. While it is always difficult to extrapolate from the laboratory to natural environments, these observations suggest that loss-of-function may be a common mode of adaptation to a new environment. This raises the question of how populations could regain such lost biological functions when the environment changes back to a prior state where that function conferred a selective advantage. This question also has great practical significance for synthetic biology, where we may be able to use evolution to resurrect evolutionarily broken synthetic biological systems in medical, environmental, or extraterrestrial applications where direct human intervention is difficult or possibly ineffective.

To this end, we investigated evolutionary reversibility by evolving 7 yeast strains with broken PF gene circuits, each with a different rtTA mutation, in conditions where regaining gene circuit function would be beneficial. The results revealed various classes of evolutionary dynamics for quasifunctional, dysfunctional, or nonfunctional mutants (Fig. 7*C*). Revertant clones arose only in dysfunctional mutant populations through extracircuit mutations. After evolving the broken PF mutants, we found no compensatory coding-sequence mutations inside the gene circuits in any populations. Instead, many new extracircuit mutations increased yEGFP::ZeoR levels, thereby improving drug resistance, without restoring broken PF function, indicating that evolution adopts alternate paths if they are available (49, 50). Restricting such alternate paths, e.g., by using higher drug concentrations or by preventing extracircuit genomic mutations (51) may facilitate functional reversions in future experiments. Importantly, some extracircuit mutations did reenable PF gene circuit function by elevating rtTA expression, indicating that evolutionary reversion is possible without any new mutations in rtTA or even the gene circuit. This is broadly consistent with another recent study that evolved *Escherichia coli* with loss-of-function mutations in a

particular enzyme, showing some direct revertant mutations in the functional locus but also indirect adaptations elsewhere in the genome (52).

We discovered interesting interactions between intracellular gene circuit dynamics, population dynamics, and evolutionary dynamics (53). Specifically, slow growth rate was not only a fitness parameter, but also a potential enabler of dynamic shifts leading to beneficial early phenotypic and later genetic changes. This is reminiscent of the emerging concept of growth rate as a global regulator of the cell's transcriptional state (54, 55). The potential implications are remarkable, since a slow-growing dysfunctional mutant can rapidly develop a large high-expression peak, appearing to be reverted. However, these early expression shifts are not truly evolutionary reversions, they simply result from gaining access to a bistable regime that existed for the entire time but was inaccessible through hyper-induction. Indeed, other conditions that decelerate growth similarly to Zeocin, ethanol, and Cisplatin could also boost bistability for such mutants. To combat drug resistance, it will be important to understand how often similar growth-related dynamic shifts (38, 39, 54) can happen in natural networks of bacteria, yeasts, and mammalian cells. Furthermore, the antibiotic's mechanism of action matters for survival and evolution. As the mathematical model suggested, stressors that reduce growth without directly interfering with protein synthesis enabled access to a bistable regime. On the other hand, antibiotics such as G418 that directly inhibit translation (43) might prevent protein expression-dependent dynamical shifts, and consequently the emergence of high-expressors. Future studies evaluating the effect of different antibiotic mechanisms of action on gene-network dynamics and evolution will be important and informative.

Sanger sequencing revealed only 1 intracircuit mutation across all different tested mutants: A 42-bp deletion eliminating the first *tetO2* operator site upstream of the *yEGFP::zeoR* coding region. The other *tetO2* site upstream from *yEGFP::zeoR* and the 2 *tetO2* sites upstream from *rtTA* remained intact, leaving positive feedback unaltered while still enabling *yEGFP::zeoR* activation by rtTA. We could not link the observed phenotypes and the identified *tetO2* site deletion specifically, except for Missense 3, where 1 *tetO2* site was absent only in monostable populations, while bistable clones had intact gene circuits. Notably, *tetO2* site deletions occurred in nonfunctional mutants and also in cells previously evolved in D0Z2 (9), suggesting that these deletions contribute to elevating basal yEGFP::zeoR expression independently of rtTA. Establishing the functional and dynamic effects of single versus double *tetO2* sites in front of *yEGFP::zeoR* requires further investigation. Extracircuit mutations in various genes, such as *SRB8*, *MED6*, *CCT7*, *NUP159*, and others suggest alterations in the transcription and protein-folding processes, which will require further studies.

Upon sorting and separately culturing low- and high-expressor subpopulations from evolving populations with quasifunctional and dysfunctional mutants, only the latter contained revertant clones that reestablished and maintained bistability. Hence, we successfully generated fully revertant clones capable of stably reactivating the mutant PF circuit. Interestingly, the reversion could be linked to an extracircuit mutation in the *SSN2* gene, pointing to functional alterations in the RNA polymerase II-mediator complex controlling transcriptional regulation, and consequently conferring drug resistance through rtTA and yEGFP::zeoR protein levels. Compared to the ancestral PF and the original Missense 3 gene circuit, the revertant strains were Zeocin-resistant (*SI Appendix*, Fig. S10) yet high expression was not costly, indicating that breaking and then recovering the gene circuit function resulted in PF cell lines with functional gene circuits that are more robust to evolution and environmental perturbations.

Fusing an antibiotic resistance cassette to genes of interest would likely be useful to restore the function of other activator-based gene circuits. The regulators of gene circuits employing only repressors (such as the toggle switch) would be less likely to degrade by evolution in eukaryotes where steric repressors tend to be less toxic than activators, so the evolutionary pressure to mutate them would be lower. Nonetheless, fusing an antibiotic resistance gene to target genes and applying drug selection should allow regaining of function even for repressor-based gene circuits if they break down. Moreover, auxotrophic positive- and negative-selection markers (such as URA3) could be similarly employed as handles for evolutionary restoration, with the advantage that selection could be applied both for low and high expression in yeast.

As opposed to our method, directed evolution studies in the past optimized enzymes and metabolic pathways (33, 34) to avoid the difficulties of rational troubleshooting and screening. Such studies focused on individual proteins, mutagenizing coding sequences and screening for optimal variants. In particular, a study titled "Directed evolution of a genetic circuit" in fact mutagenized the coding sequence of a single transcription factor and then screened for optimal variants without actually performing network evolution (33), that is, allowing the entire network and host genome to change naturally. Other studies investigated evolutionary degradation of gene circuits but did not seek to recover or improve gene circuit function by experimental evolution (9, 30).

To conclude, our results highlight the versatility of drug-resistance mechanisms, including dynamical consequences of slow growth, and exemplify how yeast and possibly mammalian (23) gene circuit evolution can reveal interesting dynamical and biological behaviors, such as host-genomic mutations repairing lost gene circuit function.

Materials and Methods

We used previously evolved (9) YPH500 haploid *S. cerevisiae* clones (α, *ura3-52*, *lys2-801*, *ade2-101*, *trp1Δ63*, *his3Δ200*, *leu2Δ1*; Stratagene) with 7 different rtTA-mutant PF synthetic gene circuits (6) stably integrated into chromosome XV near the *HIS3* locus (*SI Appendix*, Table S1). Cells were grown in SD-his-trp + 2% galactose media at 30 °C, shaking at 300 rpm.

To phenotypically characterize the 7 mutants, we performed hysteresis and hyperinduction experiments as well as slow growth rate experiments using 40 μg/mL Cisplatin, 40 μg/mL G418 or 7.5% ethanol.

To conduct the experimental evolution, 10^5 cells were resuspended into 1 mL of D2Z0 (2 μg/mL Dox) and D2Z2 (2 μg/mL Dox, 2 mg/mL Zeocin) conditions (3 replicates each) every ∼24 h. Fluorescence (BD Accuri) and cell counts (Nexcelom) were measured daily. The experiment lasted for 14 d. Missense 1, 2, and 3 populations were FACS-sorted (BD FACSAria III) at day 4. Collected low- and high-expressor subpopulations were cultured separately in D2Z2 for 12 d. Flow-cytometry (BD Accuri) and cell counts (Nexcelom) were performed daily on the sorted samples.

To assess the fitness of evolved populations in Zeocin, we collected OD600 readings in D0Z2 over 24 h. We genetically characterized evolution endpoint populations and clonal isolates through WGS and Sanger sequencing, respectively. Evolved clonal isolates were phenotyped in D2Z2. Revertant clonal isolates were phenotyped in D0Z0, D2Z0, and D0Z2, in addition to D2Z2.

Detailed protocols are included in the *SI Appendix, Supporting Materials and Methods*.

Data Availability. Data and Matlab code associated with the figures (56) and raw sequencing data (57) can be found at https://openwetware.org/wiki/CHIP:Data.

ACKNOWLEDGMENTS. We thank Rebecca C. Connor and Todd Rueb for their help in performing the FACS sorting and the flow-cytometry readings at the Stony Brook flow cytometry facility; Oleksandra Romanyshyn and Michael Tyler Guinn for facilitating the timely execution of experiments; 2 anonymous reviewers for their insightful comments; and all G.B. laboratory members for helpful discussions and feedback. This work was supported by the NIH/National Institute of General Medical Sciences Maximizing Investigator's Research Award (MIRA) Grant R35 GM122561 (to G.B.), the Laufer Center for Physical and Quantitative Biology (G.B.), and the Swiss National Science Foundation Ambizione Grant PZ00P3_180147 (to M.M.).

1. E. Kussell, S. Leibler, Phenotypic diversity, population growth, and information in fluctuating environments. *Science* **309**, 2075–2078 (2005).
2. D. M. Wolf, V. V. Vazirani, A. P. Arkin, Diversity in times of adversity: Probabilistic strategies in microbial survival games. *J. Theor. Biol.* **234**, 227–253 (2005).
3. J. A. Hill, T. R. O'Meara, L. E. Cowen, Fitness trade-offs associated with the evolution of resistance to antifungal drug combinations. *Cell Rep.* **10**, 809–819 (2015).
4. M. Eames, T. Kortemme, Cost-benefit tradeoffs in engineered lac operons. *Science* **336**, 911–915 (2012).
5. G. I. Lang, A. W. Murray, D. Botstein, The cost of gene expression underlies a fitness trade-off in yeast. *Proc. Natl. Acad. Sci. U.S.A.* **106**, 5755–5760 (2009).
6. D. Nevozhay, R. M. Adams, E. Van Itallie, M. R. Bennett, G. Balázsi, Mapping the environmental fitness landscape of a synthetic gene circuit. *PLoS Comput. Biol.* **8**, e1002480 (2012).
7. T. Kalisky, E. Dekel, U. Alon, Cost-benefit theory and optimal design of gene regulation functions. *Phys. Biol.* **4**, 229–245 (2007).
8. T. F. Cooper, D. E. Rozen, R. E. Lenski, Parallel changes in gene expression after 20,000 generations of evolution in Escherichiacoli. *Proc. Natl. Acad. Sci. U.S.A.* **100**, 1072–1077 (2003).
9. C. González *et al*., Stress-response balance drives the evolution of a network module and its host genome. *Mol. Syst. Biol.* **11**, 827 (2015).
10. E. Dekel, U. Alon, Optimality and evolutionary tuning of the expression level of a protein. *Nature* **436**, 588–592 (2005).
11. L. Tan, S. Serene, H. X. Chao, J. Gore, Hidden randomness between fitness landscapes limits reverse evolution. *Phys. Rev. Lett.* **106**, 198102 (2011).
12. J. J. Kuzdzal-Fick, L. Chen, G. Balázsi, Disadvantages and benefits of evolved unicellularity versus multicellularity in budding yeast. *Ecol. Evol.* **9**, 8509–8523 (2019).
13. A. K. Hottes *et al*., Bacterial adaptation through loss of function. *PLoS Genet.* **9**, e1003617 (2013).
14. G. I. Lang, M. M. Desai, The spectrum of adaptive mutations in experimental evolution. *Genomics* **104**, 412–416 (2014).
15. Y.-C. Xu *et al*., Adaptation and phenotypic diversification in Arabidopsis through loss-of-function mutations in protein-coding genes. *Plant Cell* **31**, 1012–1025 (2019).
16. M. J. Behe, Experimental evolution, loss-of-function mutations, and "the first rule of adaptive evolution". *Q. Rev. Biol.* **85**, 419–445 (2010).
17. N. Philippe, E. Crozat, R. E. Lenski, D. Schneider, Evolution of global regulatory networks during a long-term experiment with Escherichia coli. *BioEssays* **29**, 846–860 (2007).
18. S. Quan *et al*., Adaptive evolution of the lactose utilization network in experimentally evolved populations of Escherichia coli. *PLoS Genet.* **8**, e1002444 (2012).
19. C. Igler, M. Lagator, G. Tkačik, J. P. Bollback, C. C. Guet, Evolutionary potential of transcription factors for gene regulatory rewiring. *Nat. Ecol. Evol.* **2**, 1633–1643 (2018).
20. M. Isalan *et al*., Evolvability and hierarchy in rewired bacterial gene networks. *Nature* **452**, 840–845 (2008).
21. F. J. Poelwijk, M. G. J. de Vos, S. J. Tans, Tradeoffs and optimality in the evolution of gene regulation. *Cell* **146**, 462–470 (2011).
22. Z. Bódi *et al*., Phenotypic heterogeneity promotes adaptive evolution. *PLoS Biol.* **15**, e2000644 (2017).
23. K. S. Farquhar *et al*., Role of network-mediated stochasticity in mammalian drug resistance. *Nat. Commun.* **10**, 2766 (2019).
24. T. S. Bayer, Using synthetic biology to understand the evolution of gene expression. *Curr. Biol.* **20**, R772–R779 (2010).
25. T. S. Gardner, C. R. Cantor, J. J. Collins, Construction of a genetic toggle switch in Escherichia coli. *Nature* **403**, 339–342 (2000).
26. M. B. Elowitz, S. Leibler, A synthetic oscillatory network of transcriptional regulators. *Nature* **403**, 335–338 (2000).
27. A. Becskei, L. Serrano, Engineering stability in gene networks by autoregulation. *Nature* **405**, 590–593 (2000).
28. C. J. Bashor, J. J. Collins, Understanding biological regulation through synthetic biology. *Annu. Rev. Biophys.* **47**, 399–423 (2018).
29. G. M. Church, M. B. Elowitz, C. D. Smolke, C. A. Voigt, R. Weiss, Realizing the potential of synthetic biology. *Nat. Rev. Mol. Cell Biol.* **15**, 289–294 (2014).
30. S. C. Sleight, B. A. Bartley, J. A. Lieviant, H. M. Sauro, Designing and engineering evolutionary robust genetic circuits. *J. Biol. Eng.* **4**, 12 (2010).
31. F. Wu, D. J. Menn, X. Wang, Quorum-sensing crosstalk-driven synthetic circuits: From unimodality to trimodality. *Chem. Biol.* **21**, 1629–1638 (2014).
32. T. Ellis, X. Wang, J. J. Collins, Diversity-based, model-guided construction of synthetic gene networks with predicted functions. *Nat. Biotechnol.* **27**, 465–471 (2009).
33. Y. Yokobayashi, R. Weiss, F. H. Arnold, Directed evolution of a genetic circuit. *Proc. Natl. Acad. Sci. U.S.A.* **99**, 16587–16591 (2002).
34. C. Schmidt-Dannert, D. Umeno, F. H. Arnold, Molecular breeding of carotenoid biosynthetic pathways. *Nat. Biotechnol.* **18**, 750–753 (2000).
35. R. P. Bennett, C. A. Cox, J. P. Hoeffler, Fusion of green fluorescent protein with the Zeocin-resistance marker allows visual screening and drug selection of transfected eukaryotic cells. *Biotechniques* **24**, 478–482 (1998).
36. A. Gatignol, H. Durand, G. Tiraby, Bleomycin resistance conferred by a drug-binding protein. *FEBS Lett.* **230**, 171–175 (1988).
37. M. Oliva-Trastoy, M. Defais, F. Larminat, Resistance to the antibiotic Zeocin by stable expression of the Sh ble gene does not fully suppress Zeocin-induced DNA cleavage in human cells. *Mutagenesis* **20**, 111–114 (2005).
38. J. B. Deris *et al*., The innate growth bistability and fitness landscapes of antibiotic-resistant bacteria. *Science* **342**, 1237435 (2013).
39. C. Tan, P. Marguet, L. You, Emergent bistability by a growth-modulating positive feedback circuit. *Nat. Chem. Biol.* **5**, 842–848 (2009).
40. S. Dasari, P. B. Tchounwou, Cisplatin in cancer therapy: Molecular mechanisms of action. *Eur. J. Pharmacol.* **740**, 364–378 (2014).
41. D. C. Eustice, J. M. Wilhelm, Mechanisms of action of aminoglycoside antibiotics in eucaryotic protein synthesis. *Antimicrob. Agents Chemother.* **26**, 53–60 (1984).
42. R. L. Adams, L. J. Terry, S. R. Wente, Nucleoporin FG domains facilitate mRNP remodeling at the cytoplasmic face of the nuclear pore complex. *Genetics* **197**, 1213–1224 (2014).
43. T. Borggrefe, R. Davis, H. Erdjument-Bromage, P. Tempst, R. D. Kornberg, A complex of the Srb8, -9, -10, and -11 transcriptional regulatory proteins from yeast. *J. Biol. Chem.* **277**, 44202–44207 (2002).
44. Y. C. Lee, S. Min, B. S. Gim, Y. J. Kim, A transcriptional mediator protein that is required for activation of many RNA polymerase II promoters and is conserved from yeast to humans. *Mol. Cell. Biol.* **17**, 4622–4632 (1997).
45. Y. Takagi, R. D. Kornberg, Mediator as a general transcription factor. *J. Biol. Chem.* **281**, 80–89 (2006).
46. V. Stoldt *et al*., Review: The Cct eukaryotic chaperonin subunits of Saccharomyces cerevisiae and other yeasts. *Yeast* **12**, 523–529 (1996).
47. M. M. Luke *et al*., The SAP, a new family of proteins, associate and function positively with the SIT4 phosphatase. *Mol. Cell. Biol.* **16**, 2744–2755 (1996).
48. C. Cappellaro, V. Mrsa, W. Tanner, New potential cell wall glucanases of Saccharomyces cerevisiae and their involvement in mating. *J. Bacteriol.* **180**, 5030–5037 (1998).
49. S. Kim, T. D. Lieberman, R. Kishony, Alternating antibiotic treatments constrain evolutionary paths to multidrug resistance. *Proc. Natl. Acad. Sci. U.S.A.* **111**, 14494–14499 (2014).
50. F. J. Poelwijk, D. J. Kiviet, D. M. Weinreich, S. J. Tans, Empirical fitness landscapes reveal accessible evolutionary paths. *Nature* **445**, 383–386 (2007).
51. A. Chavez *et al*., Precise Cas9 targeting enables genomic mutation prevention. *Proc. Natl. Acad. Sci. U.S.A.* **115**, 3669–3673 (2018).
52. J. V. Rodrigues, E. I. Shakhnovich, Adaptation to mutational inactivation of an essential gene converges to an accessible suboptimal fitness peak. *eLife* **8**, e50509 (2019).
53. A. Sanchez, J. Gore, Feedback between population and evolutionary dynamics determines the fate of social microbial populations. *PLoS Biol.* **11**, e1001547 (2013).
54. A. Y. Weiße, D. A. Oyarzún, V. Danos, P. S. Swain, Mechanistic links between cellular trade-offs, gene expression, and growth. *Proc. Natl. Acad. Sci. U.S.A.* **112**, E1038–E1047 (2015).
55. M. Scott, C. W. Gunderson, E. M. Mateescu, Z. Zhang, T. Hwa, Interdependence of cell growth and gene expression: Origins and consequences. *Science* **330**, 1099–1102 (2010).
56. M. K. Gouda, G. Balázsi, Flow cytometry and cell count data. Google Drive. https://drive.google.com/drive/folders/13jrR8XHP4p96-bcNGTlxRpFzjTfRvPkh. Deposited 16 October 2019.
57. M. K. Gouda, G. Balázsi, Raw whole-genome sequencing (WGS) data. Google Drive. https://drive.google.com/drive/folders/1sZxfXY-AzigYSCDhX_SW0bSNqfgo72lh. Deposited 16 October 2019.

Supporting Information:

Evolutionary regain of lost gene circuit function

Mirna Kheir Gouda[1,2], Michael Manhart[3] and Gábor Balázsi[1,2]

[1]The Louis and Beatrice Laufer Center for Physical and Quantitative Biology, Stony Brook University, Stony Brook, New York, 11794-5252, USA

[2]Department of Biomedical Engineering, Stony Brook University, Stony Brook, New York, 11794-5281, USA

[3]Institute of Integrative Biology, Eidgenössische Technische Hochschule (ETH) Zürich, 8092 Zürich, Switzerland

Table of contents

www.pnas.org/cgi/doi/10.1073/pnas.1912257116

1. Supporting Materials and Methods

Yeast strains

We used previously evolved [1] YPH500 haploid *Saccharomyces cerevisiae* clones (α, ura3-52, lys2-801, ade2-101, trp1Δ63, his3Δ200, leu2Δ1; Stratagene) with wild-type and seven rtTA-mutant PF synthetic gene circuits [2] stably integrated into chromosome XV near the *HIS3* locus (Table S1). A 2% weight of galactose Synthetic Dropout (SD) culture medium with appropriate supplements (-his, -trp) was used to maintain auxotrophic selection (all reagents from Sigma). Cells were grown in SD-his-trp + 2% galactose plus Doxycycline and Zeocin as indicated at 30°C, shaking at 300 rpm (LabNet 311DS shaking incubator).

Experimental evolution

Previously [1], mutant strains were isolated and stored in 27% glycerol (Thermo Fisher Scientific) at -80C. Seven mutant strains were picked from the -80C stock, streaked onto SD -his -trp 2% glucose plates (all reagents from Sigma) and incubated at 30ºC for 2 days. One isolated colony from each plate was cultured in liquid SD -his -trp 2% galactose media at 30ºC & 300rpm for 24 hours. For each strain, 10^5 cells were resuspended into 1mL of D2Z0 (2 μg/mL Doxycycline) and D2Z2 (2 μg/mL Doxycycline (Thermo Fisher Scientific), 2mg/mL Zeocin (Thermo Fisher Scientific)) conditions (3 replicates each) every ~24h. Fluorescence (BD Accuri™) and cell counts (Nexcelom) were measured daily. The experiment lasted for 14 days.

Cell Sorting

Missense 1, 2 and 3 populations were FACS-sorted at day 4 using the BD FACSAria™ III. Sorting parameters were set on the BD FACSDiva™ 8.0 software. High-sorted cells were collected from the highest 5-10% of the high-expressor subpopulations. Collected low- and high-expressor subpopulations were cultured separately in D2Z2 for 12 days. Flow-cytometry (BD Accuri™) and cell counts (Nexcelom) were performed daily on the sorted samples.

Flow-cytometry

The BD FACSAria™ III at the Stony Brook Flow-cytometry facility was used for cell sorting.

The BD Accuri™ C6 flow-cytometer was used to collect data for hyperinduction, experimental evolution for sorted and unsorted populations.

The BD FACSCalibur™ at the Stony Brook Flow-cytometry facility was used to collect data for slow growth rate and phenotyping experiments.

Estimation of population fitness

We counted cells daily using the Nexcelom Bioscience Cellometer Vision cell counter. The daily (T=24h) resuspension of a low number of cells (10^5) ensures that cells remain in the exponential growth phase throughout these experiments. Therefore, based on Nexcelom cell counts before each resuspension, we can use the exponential growth equation to estimate the population growth rate, r : $r = \frac{1}{T}\ln\left(\frac{N(t)}{N_0}\right)$.

Hyperinduction and slow growth rate experiments

To classify quasifunctional, dysfunctional and nonfunctional rtTA mutants, we cultured them in 6 µg/mL (D6Z0) or 8 µg/mL (D8Z0) Doxycycline (Thermo Fisher Scientific) added to SD-his-trp for 24h. Flow-cytometry (BD Accuri™) was performed to measure gene expression levels.

To assess the effect of slow growth rate on mutant and ancestral PF circuit dynamics, we cultured mutant (Missense 1, 2, 3, Nonsense and Deletion) and ancestral PF strains in 2 µg/mL Doxycycline (D2Z0) +7.5% 200 proof ethanol (Pharmco) for 4 days. Cells were resuspended at a 10^5 cells/mL density every day. We measured cell counts daily and protein expression by flow-cytometry on days 1, 2 and 4 (BD FACSCalibur™). Additionally, we conducted the same experiment using Cisplatin (Selleckchem) and G418 (Gemini Bio-products), each at a concentration of 40µg/mL.

Zeocin only growth curve monitoring

Original mutants and evolved replicates were cultured in the D0Z2 (2mg/mL Zeocin (Thermo Fisher Scientific)) condition at a concentration of 10^5 cells/mL. Growth curves were monitored through OD600 measurements (every 20 minutes for 24 hours) using the Tecan Infinite® 200 PRO plate reader. The following strains were monitored in D0Z2:

- Original (unevolved) ancestor strains of each mutant.
- Replicate 3 (WGS replicate) of evolved populations of each mutant, from day 14 of experimental evolution, except for Missense 3 where all replicates were tested.
- Sequenced and phenotyped clonal isolates (shown in Tables S3-S5) for each mutant.

In addition, for control and comparison purposes, we monitored the growth of ancestral PF in D0Z0, D2Z2 and D0Z2.

DNA isolation

DNA was extracted from isolated single clones for Sanger sequencing or from evolved populations for WGS using the MasterPure™ Yeast DNA Purification Kit (Lucigen) as per manufacturer's instructions.

Sanger sequencing

Sanger sequencing was performed on 10 isolated evolved clones from each unsorted mutant population at day 14 and 5 isolated clones from the sorted revertant Missense 3 replicate at day 12. For primers, see SI Appendix, Table S2. Samples were sequenced at the DNA Sequencing Facility at Stony Brook University using the BigDye Terminator v3.1 sequencing kit, BigDye XTerminator Purification kit and the 3730 DNA Analyzer (all from Applied Biosystems). Results were analyzed using the SnapGene software sequence alignment tool.

Whole genome sequencing (WGS) analysis

WGS was performed on Missense 1 r3, Missense 2 r3 and Missense 3 r1 and r3 at days 1, 3 and 14 for unsorted populations and days 1, 5 and 12 for the sorted populations. WGS was also performed on r3 of each of the other mutants on day 14 only. Samples were sent to Novogene Co., Ltd. where library preparation was performed using the NEBNext® Ultra II kit (New England Biolabs) and sequencing was performed by Illumina HiSeq-4000 at a 165x coverage.

To analyze the sequencing data, we used the S288C genome (RefSeq accession numbers NC_001133.9, NC_001134.8, NC_001135.5, NC_001136.10, NC_001137.3, NC_001138.5, NC_001139.9, NC_001140.6, NC_001141.2, NC_001142.9, NC_001143.9, NC_001144.5, NC_001145.3, NC_001146.8, NC_001147.6, NC_001148.4, NC_001224.1) as a reference with the PF circuit inserted computationally on chromosome 15 between the MRM1 and HIS3 genes. We processed the reads and this modified reference genome using the breseq 0.33.1 pipeline on default settings for polymorphism prediction [3]. The pipeline produced lists of inferred variants (including SNPs, insertions, and deletions) and their estimated frequencies in the population for each sequencing sample. Subsequently, inferred variants were filtered down according to the following three criteria: (i). Variant cannot appear in samples from different populations (e.g., Missense 1 and Missense 3). (ii).Variant must appear in multiple samples if it appears in a population with multiple samples. (iii).Variant must appear >10% in at least one sample.

Here we highlight mutations as potentially causal if they increase in frequency over time or if they are absent at the beginning but are detected in high frequencies (>50%) at the end of the evolution experiment. All detected variants are reported (Datasets S1-S7).

Phenotyping of isolated clones

To understand the effect of the *tetO2* deletion detected upstream of *yEGFP::zeoR* by Sanger sequencing on PF dynamics, one clone from each PF genotype found (presence of *tetO2* or deletion of *tetO2*) was cultured in D2Z2 for 24h. Flow-cytometry was performed to obtain a protein expression distribution (BD FACSCalibur™).

To compare PF to the revertant Missense 3 r1 mutant (revertant), PF and the five Sanger-sequenced revertant clones were cultured in D0Z0, D2Z0, D2Z2 and D0Z2 for 4 days. Flow-cytometry was performed to obtain a protein expression distribution on each day (BD FACSCalibur™).

Quantitative modeling and software

Flow cytometry data were gated based on forward and side scatter using FCS Express and then exported for subsequent analysis. All experimental data were analyzed and plotted in MATLAB R2016b. WGS data were analyzed using the breseq 0.33.1 software. Ordinary differential equation (ODE) models were developed, then their steady states were analyzed on paper and by custom-written scripts using the function *roots* in MATLAB R2018a. See the SI model for details.

Yeast sample storage for further analysis

Each day, unsorted and sorted samples from the experimental evolution and were stored in 27% glycerol at -80C for further studies. Sanger sequenced clones and whole genome sequenced clones were also stored in 27% glycerol.

2. Supporting Tables and Datasets

Mutant	Position in rtTA	Position in S288C+PF chr15	Nucleotide effect	Amino acid effect	Phenotypic effect	Evolved population: Gonzalez et al., 2015
Missense 1	189	729,794	C→G	His→Gln	Quasifunctional	D2Z0-12hr-r2
Missense 2	562	730,167	T→C	Phe→Leu	Quasifunctional	D2Z0-24hr-r2
Missense 3	275	729,880	G→A	Ser→Asn	Dysfunctional	D2Z0-24hr-r3
Missense 4	13	729,618	G→T	Asp→Tyr	Nonfunctional	D2Z0-24hr-r3
Nonsense	442	730,047	G→T	Glu→Stop	Nonfunctional	D2Z0-24hr-r2
Deletion	651	730,256	78bp deletion	26 amino acid deletion	Nonfunctional	D2Z0-24hr-r3
Duplication	95	729,700	30bp duplication	10 amino acid duplication	Nonfunctional	D2Z0-24hr-r1

Table S1. Genotypes of the 7 mutants before the evolution experiment.

Primer name	Sequence
TRP-f	ATGTCTGTTATTAATTTCACAGGTAGTTC
rtTA-seq-int-r-cg	CGACTTGATGCTCTTGTTCTTCCAATACGCAACC
rtTA-seq-int-f-cg	GCCAACAAGGTTTTTCACTAGAGAATGCATTATATG
Tetreg-AflII-f	GCGCCTTAAGGCGCCACTTCTAAATAAGCGAATTTC
rtTABamHI2-f	GCGCGGATCCATGTCTAGATTAGATAAAAGTAAAG
FFF-XhoI-r	GCGCCTCGAGTTAACCTGGCAACATATCTAAATCAAAGTCATC
Backbone-r	CGCGTTGGCCGATTCATTAATGC
His-f	ATGACAGAGCAGAAAGCCCTAGTAAAGC
ZeoR-XhoI-r	GCGCCTCGAGTCAGTCCTGCTCCTC

Table S2. Sanger sequencing primers for the PF gene circuit region.

Mutant ancestor	Genomic mutations		Frequency of genomic mutations at day 14	*tetO2* deletion freq. in 10 clones	Single clone phenotypes in D2Z2 (24h)
Missense 1 r3	Phospholipid biosynthesis	*PAH1* T479P (ACG→CCG) (Thr→Pro)	14.3%	10/10	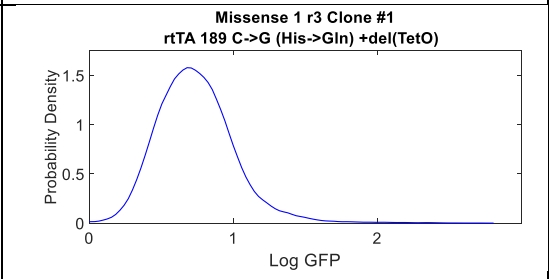
	Histone-binding	*SET3* coding (440/2256 nt) Δ1 bp	14.5%		
		SET3 G147S (GGC→AGC) (Gly→Ser)	14.4%		
Missense 2 r3	Mitochondrial metabolism	*Phb2* Y138N (TAC→AAC) (Tyr→Asn)	100%	0/10	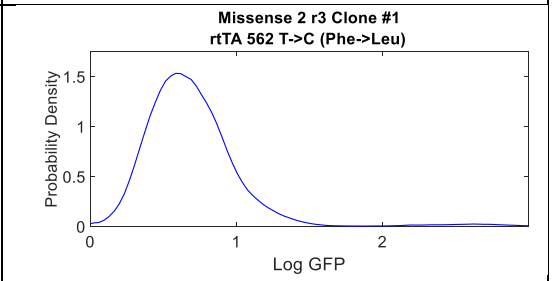
		Mdm32 S142C (AGC→TGC) (Ser→Cys)	100%		
		COX1 Intragenic (+762/-125) Δ1bp	100%		
	Transcriptional regulation	*NUP159* A615A (GCA→GCC) Synonymous Ala	100%		

Table S3. Genotyping and phenotyping of individual clones evolved from quasifunctional mutants Missense 1 and Missense 2. Genomic mutations reported here arose during the 14-day evolution experiment.

Mutant ancestor	*tetO2* deletion freq. in 10 clones	Single clone phenotypes in D2Z2 (24h)
Missense 4 r3	0/10	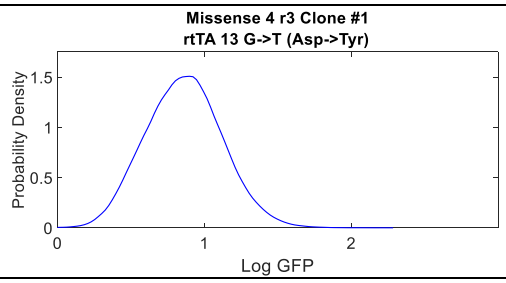
Nonsense r3	1/10	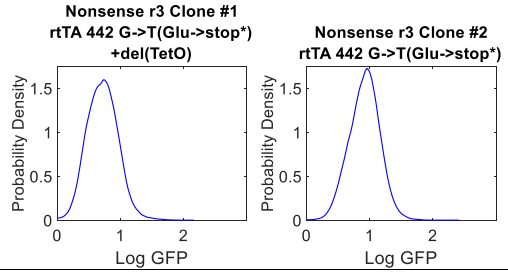
Deletion r3	8/10	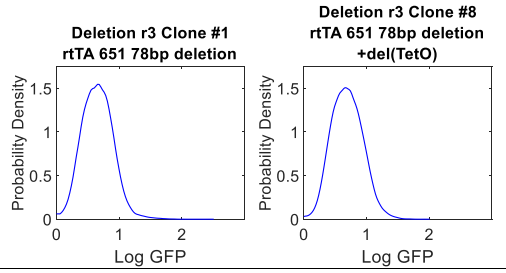
Duplication r3	2/10	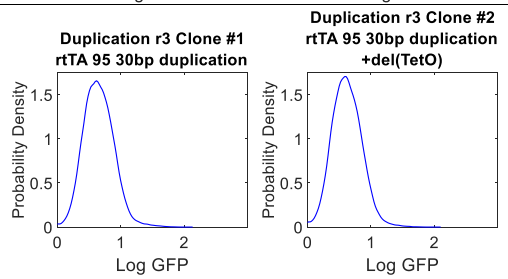

Table S4. Genotyping and phenotyping of individual clones evolved from nonfunctional mutants Missense 4, Nonsense, Deletion and Duplication. Mutations reported here arose during the 14-day evolution experiment.

Mutant ancestor	Genomic mutations		Frequency of genomic mutations at day 14	*tetO2* deletion freq. in 10 clones	Single clone phenotypes in D2Z2 (24h)
Missense 3 r1	Chromatin regulation	*SIF2* coding (144/1608 nt) Δ1 bp	32.6%	4/10	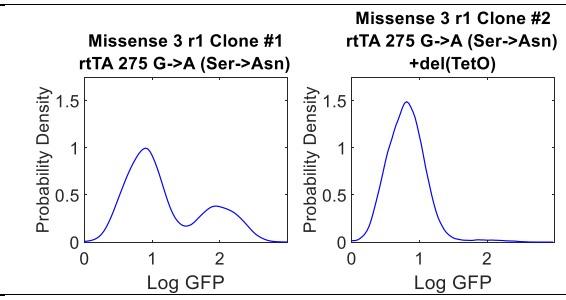
	Transcriptional regulation	*SSN2* V239D (GTT→GAT) Val→Asp	5.6%		
	Transcriptional regulation	*SSN3* coding (47/1668 nt) Δ1 bp	34.4%		
Missense 3 r2	Not sequenced by WGS			10/10	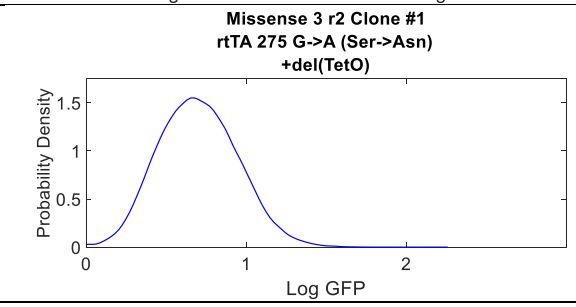
Missense 3 r3	Transcriptional regulation	*SRB8* P116R (CCT→CGT) (Pro →Arg)	100%	0/10	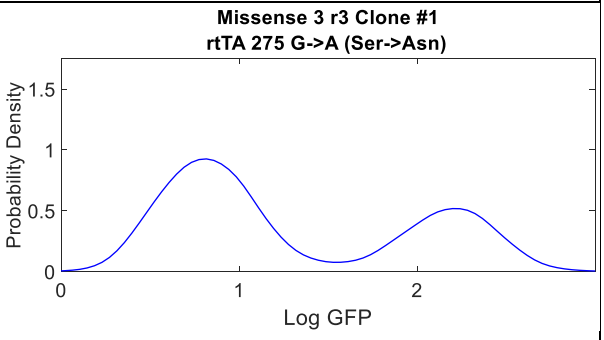
		MED6 Y100F (TAT→TTT) (Tyr→Phe)	100%		
	Protein folding	*CCT7* R469S (AGA→AGT)	100%		
	Cell Cycle	*SAP185* coding (423/3177 nt) Δ1bp	100%		
		ECM38 →/→ *EXG1* intergenic (+634/-270) (T→A)	100%		

Table S5. Genotyping and phenotyping of individual clones evolved from dysfunctional mutant Missense 3. Genomic mutations reported here arose during the 14-day evolution experiment.

List of Whole Genome Sequencing Datasets:

Dataset S1. WGS variants for Missense 1, replicate 3.

Dataset S2. WGS variants for Missense 2, replicate 3.

Dataset S3. WGS variants for Missense 3, replicates 1 and 3.

Dataset S4. WGS variants for Missense 4, replicate 3.

Dataset S5. WGS variants for Nonsense, replicate 3.

Dataset S6. WGS variants for Deletion, replicate 3.

Dataset S7. WGS variants for Duplication, replicate 3.

3. Supporting Figures

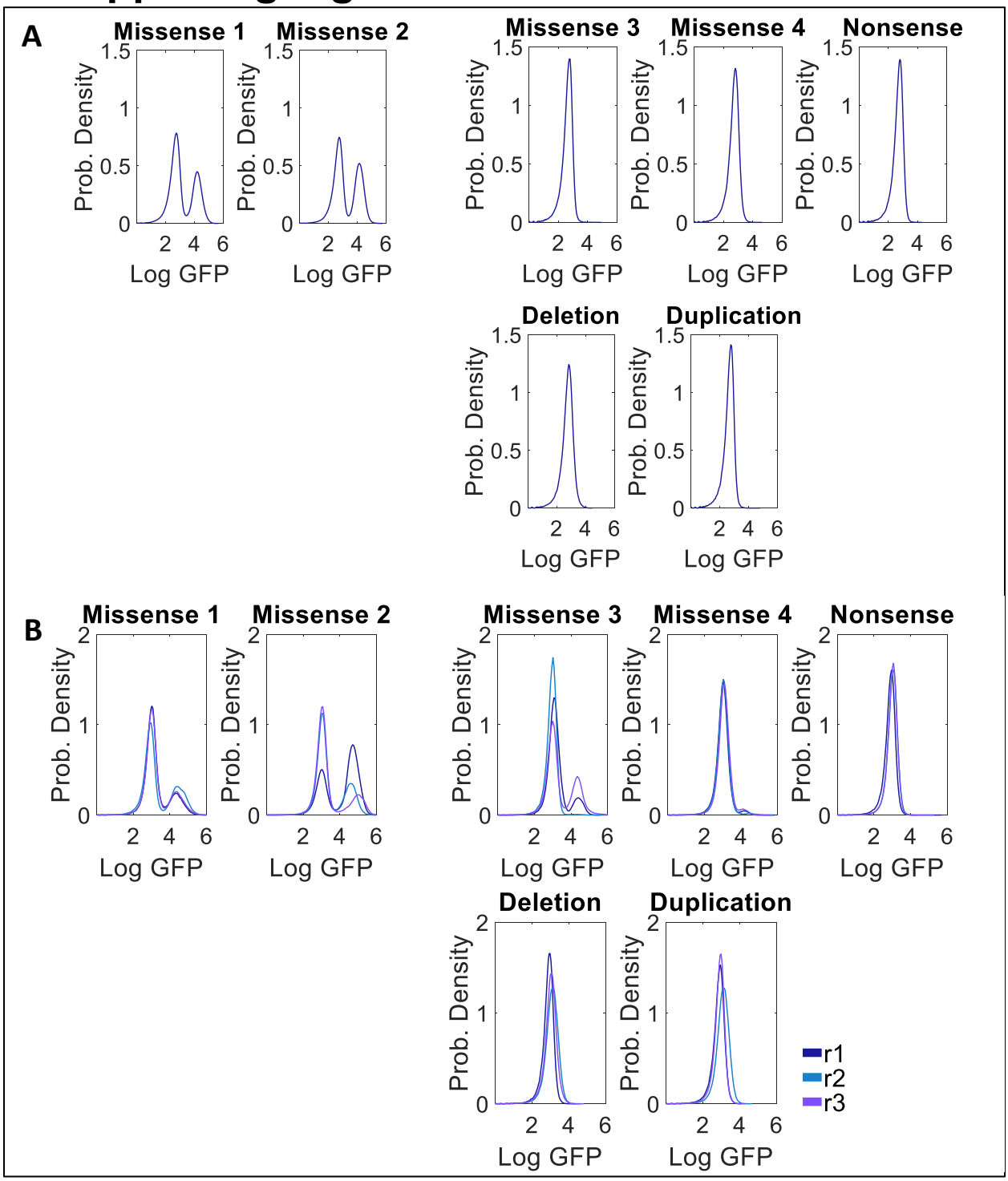

Figure S1. (A) Hyper-induction of original mutants in D8Z0 prior to the evolution experiment. (B) Hyper-induction of evolved mutants in D8Z0 following the evolution experiment.

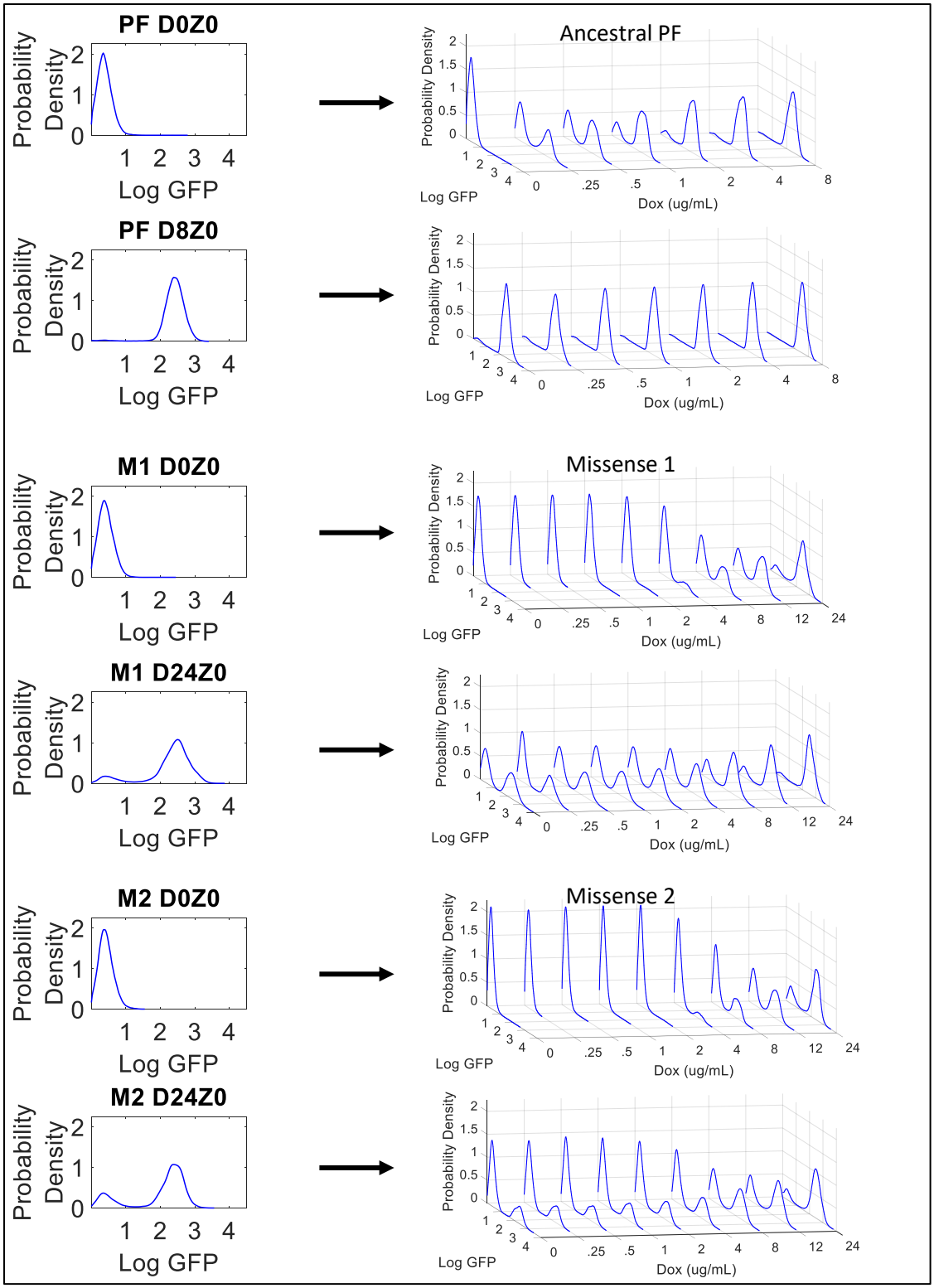

Figure S2. Hysteresis experiments showing the difference in Dox dose response of Missense 1 and 2 gene circuits versus the ancestral PF gene circuit within 1 day (to minimize the chance of mutations). Defining bistability based on high expressors after transfer, we obtain the ranges to be [0.05 – 8] μg/mL for ancestral PF, and [2 - 24] μg/mL for Missense 1 and 2.

A

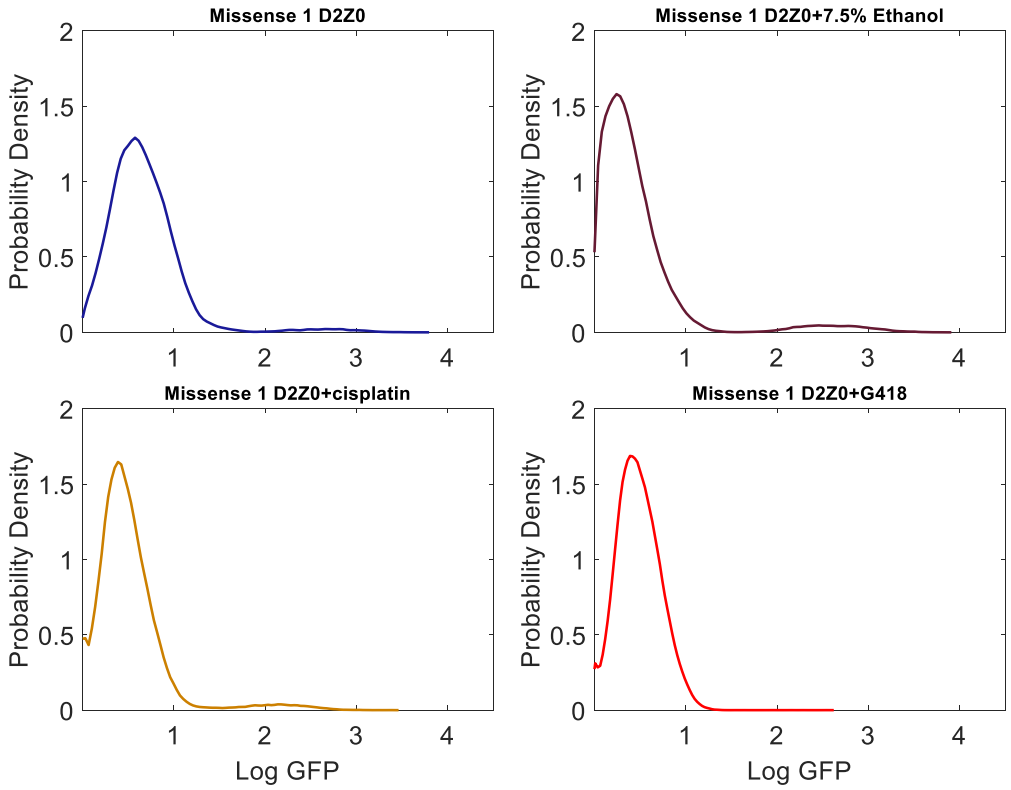

B

Missense 1 D2Z0 g=0.284			
Subpop.	**# of events**	**Percentage**	**Geometric mean**
High GFP	**2033**	**1.85%**	**198.97**
Low GFP	**107754**	**98.14%**	**3.42**
Missense 1 D2Z0 + 7.5% EtOH g=0.098			
Subpop.	**# of events**	**Percentage**	**Geometric mean**
High GFP	**4437**	**4.06%**	**185.85**
Low GFP	**104935**	**95.92%**	**1.89**
Missense 1 D2Z0 + Cisplatin (40ug/mL) g=0.093			
Subpop.	**# of events**	**Percentage**	**Geometric mean**
High GFP	**3563**	**3.24%**	**137.89**
Low GFP	**106427**	**96.76%**	**2.88**
Missense 1 D2Z0 + G418 (40ug/mL) g=0.093			
Subpop.	**# of events**	**Percentage**	**Geometric mean**
High GFP	**4**	**0.00%**	**171.54**
Low GFP	**109986**	**100.00%**	**3.05**

Figure S3. Effect of slow growth rate due to ethanol and Cisplatin on Missense 1 distributions in D2Z0 at day 4. (A) Gene expression distributions. (B) Histogram statistics.

A

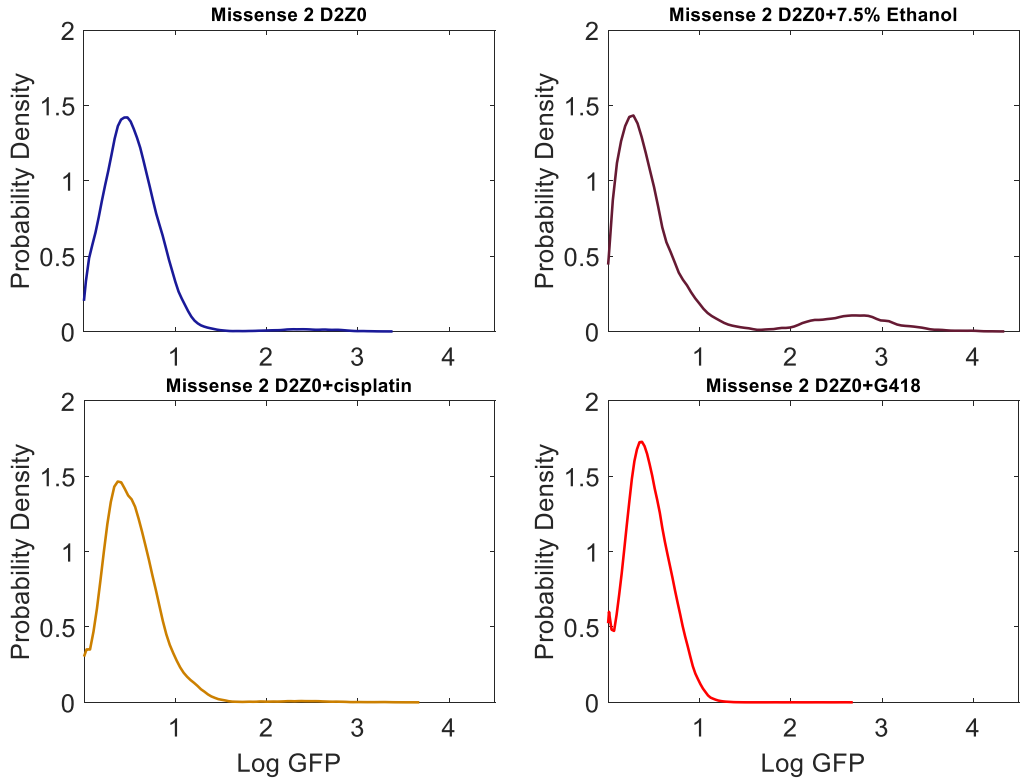

B

Missense 2 D2Z0 g=0.269			
Subpop.	**# of events**	**Percentage**	**Geometric mean**
High GFP	**1204**	**1.10%**	**131.32**
Low GFP	**108599**	**98.90%**	**2.67**
Missense 2 D2Z0 + 7.5% EtOH g=0.052			
Subpop.	**# of events**	**Percentage**	**Geometric mean**
High GFP	**2503**	**9.97%**	**217.84**
Low GFP	**22578**	**89.94%**	**2.09**
Missense 2 D2Z0 + Cisplatin (40ug/mL) g=0.127			
Subpop.	**# of events**	**Percentage**	**Geometric mean**
High GFP	**803**	**0.73%**	**261.61**
Low GFP	**108746**	**99.27**	**3.30**
Missense 2 D2Z0 + G418 (40ug/mL) g=0.138			
Subpop.	**# of events**	**Percentage**	**Geometric mean**
High GFP	**8**	**0.01%**	**181.26**
Low GFP	**109880**	**99.99%**	**2.74**

Figure S4. Effect of slow growth rate due to ethanol and Cisplatin on Missense 2 distributions in D2Z0 at day 4. (A) Gene expression distributions. (B) Histogram statistics.

A

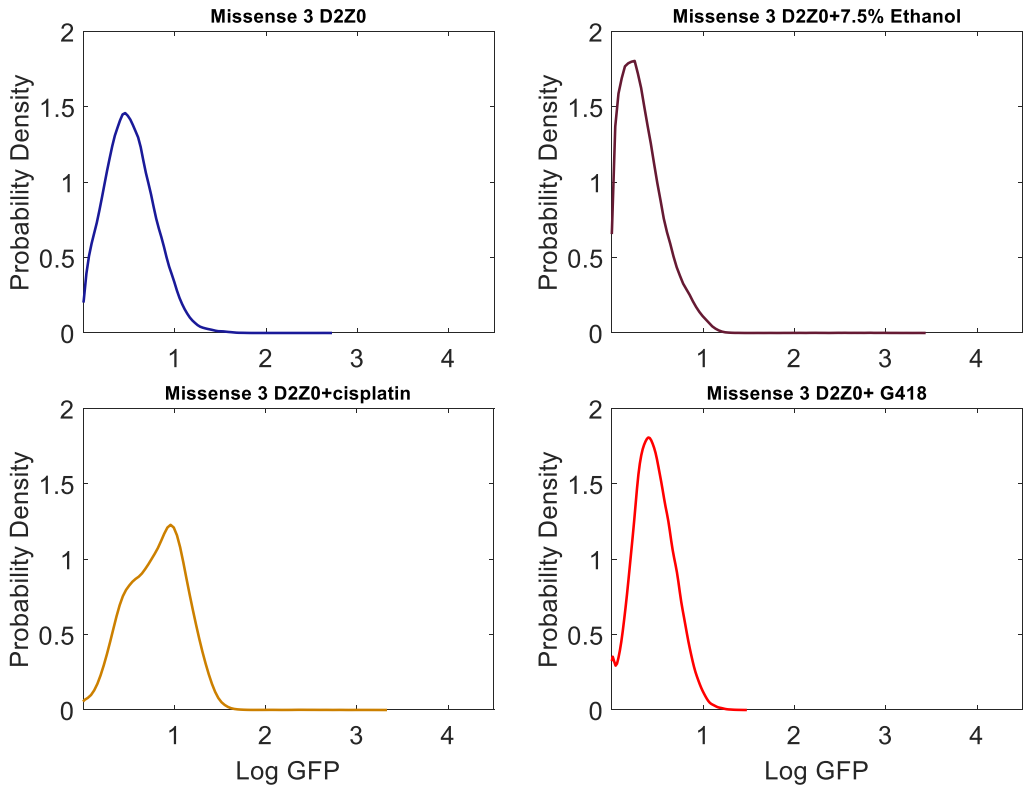

B

Missense 3 D2Z0 g=0.266			
Subpop.	**# of events**	**Percentage**	**Geometric mean**
High GFP	**0**	**0.00%**	**N/A**
Low GFP	**109892**	**100.00%**	**2.65**
Missense 3 D2Z0 + 7.5% EtOH g=0.048			
Subpop.	**# of events**	**Percentage**	**Geometric mean**
High GFP	**74**	**0.07%**	**157.30**
Low GFP	**108200**	**99.93%**	**1.77**
Missense 3 D2Z0 + Cisplatin (40ug/mL) g=0.079			
Subpop.	**# of events**	**Percentage**	**Geometric mean**
High GFP	**52**	**0.09%**	**222.44**
Low GFP	**57908**	**99.91%**	**6.31**
Missense 3 D2Z0 + G418 (40ug/mL) g=0.115			
Subpop.	**# of events**	**Percentage**	**Geometric mean**
High GFP	**0**	**0.00%**	**N/A**
Low GFP	**109958**	**100.00%**	**2.89**

Figure S5. Effect of slow growth rate due to ethanol and Cisplatin on Missense 3 distributions in D2Z0 at day 4. (A) Gene expression distributions. (B) Histogram statistics.

A

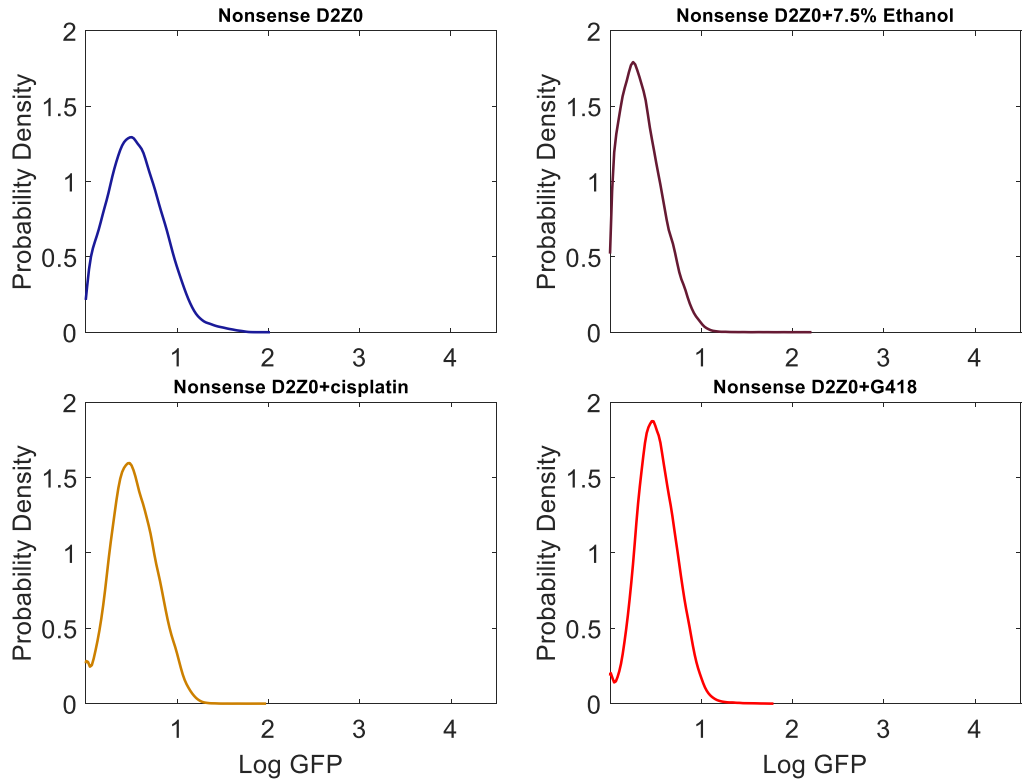

B

Nonsense D2Z0 g=0.278			
Subpop.	**# of events**	**Percentage**	**Geometric mean**
High GFP	**0**	**0.00%**	**N/A**
Low GFP	**109786**	**100.00%**	**2.80**
Nonsense D2Z0 + 7.5% EtOH g=0.071			
Subpop.	**# of events**	**Percentage**	**Geometric mean**
High GFP	**4**	**0.00%**	**54.00**
Low GFP	**98914**	**100.00%**	**1.85**
Nonsense D2Z0 + Cisplatin (40ug/mL) g=0.185			
Subpop.	**# of events**	**Percentage**	**Geometric mean**
High GFP	**0**	**0.00%**	**N/A**
High GFP	**106642**	**100.00%**	**3.37**
Nonsense D2Z0 + G418 (40ug/mL) g=0.184			
Subpop.	**# of events**	**Percentage**	**Geometric mean**
High GFP	**0**	**0.00%**	**N/A**
Low GFP	**102878**	**100.00%**	**3.28**

Figure S6. Effect of slow growth rate due to ethanol and Cisplatin on Nonsense distributions in D2Z0 at day 4. (A) Gene expression distributions. (B) Histogram statistics.

A

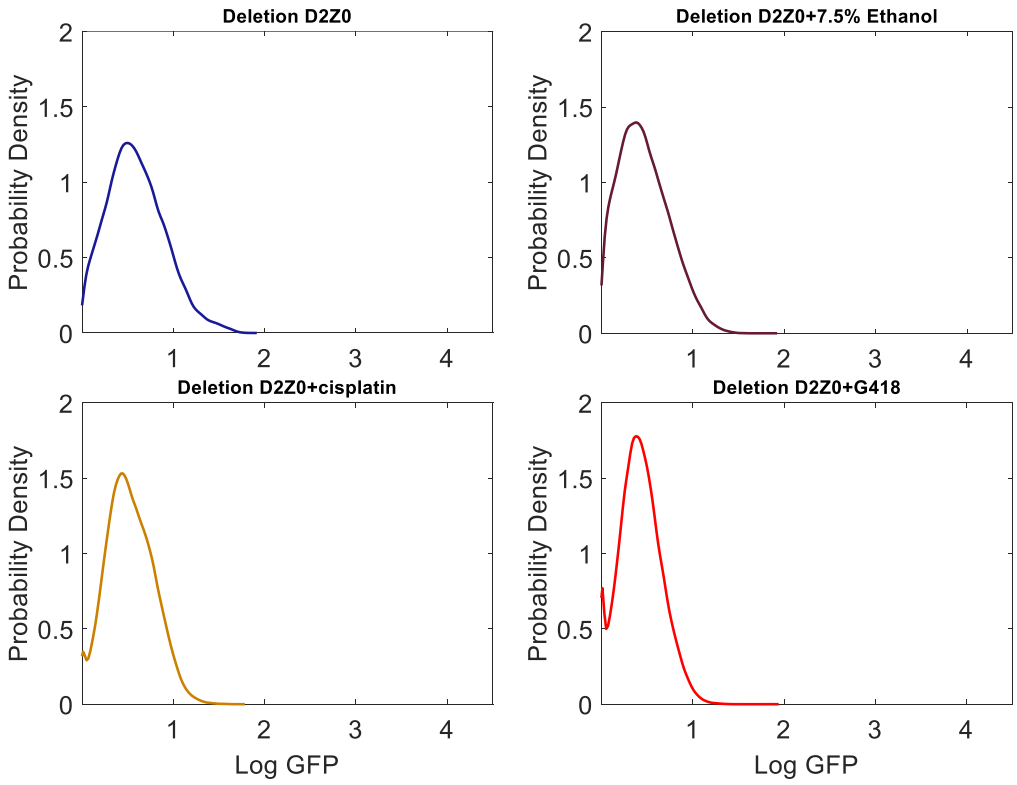

B

Deletion D2Z0 g=0.287			
Subpop.	**# of events**	**Percentage**	**Geometric mean**
High GFP	**0**	**0.00%**	**N/A**
Low GFP	**109290**	**100.00%**	**3.06**
Deletion D2Z0 + 7.5% EtOH g=0.130			
Subpop.	**# of events**	**Percentage**	**Geometric mean**
High GFP	**0**	**0.00%**	**N/A**
Low GFP	**109887**	**100.00%**	**2.35**
Deletion D2Z0 + Cisplatin (40ug/mL) g=0.084			
Subpop.	**# of events**	**Percentage**	**Geometric mean**
High GFP	**0**	**0.00%**	**N/A**
Low GFP	**109765**	**100.00%**	**3.35**
Deletion D2Z0 + G418 (40ug/mL) g=0.084			
Subpop.	**# of events**	**Percentage**	**Geometric mean**
High GFP	**0**	**0.00%**	**N/A**
Low GFP	**109951**	**100.00%**	**2.66**

Figure S7. Effect of slow growth rate due to ethanol and Cisplatin on Deletion distributions in D2Z0 at day 4. (A) Gene expression distributions. (B) Histogram statistics

A

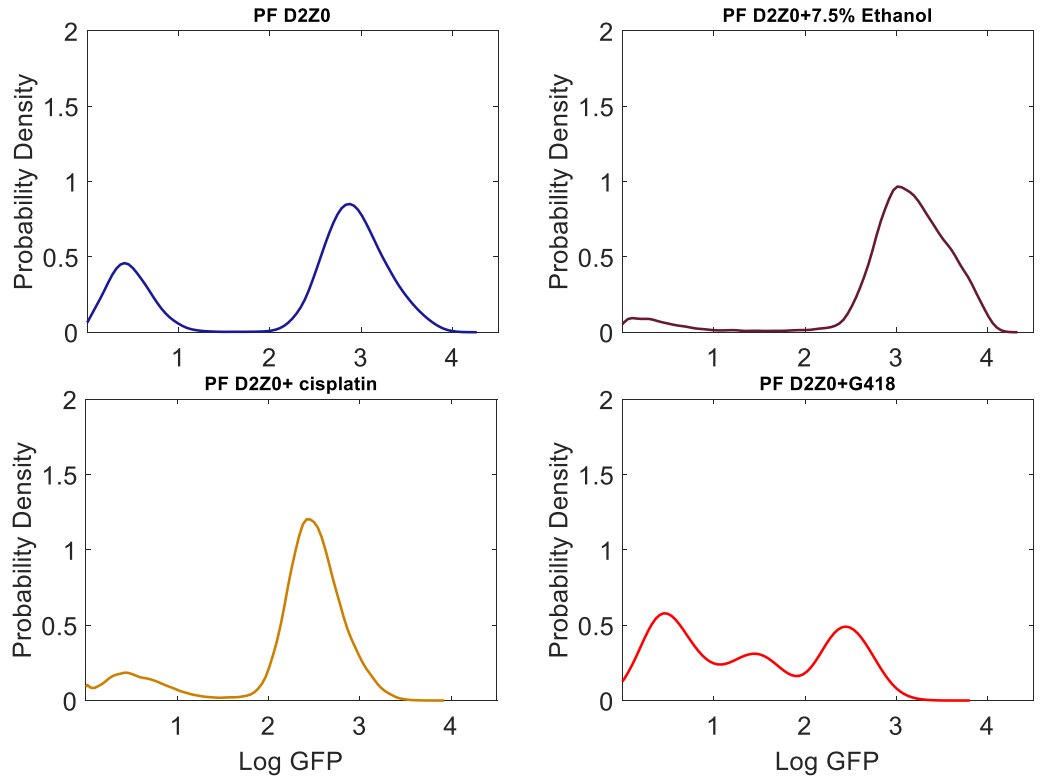

B

PF D2Z0 g=0.146			
Subpop.	**# of events**	**Percentage**	**Geometric mean**
High GFP	**77456**	**71.02%**	**359.03**
Low GFP	**31588**	**28.96%**	**2.49**
PF D2Z0 + 7.5% EtOH g=0.046			
Subpop.	**# of events**	**Percentage**	**Geometric mean**
High GFP	**29216**	**90.70%**	**584.10**
Low GFP	**2986**	**9.27%**	**2.02**
PF D2Z0 + Cisplatin (40ug/mL) g=0.107			
Subpop.	**# of events**	**Percentage**	**Geometric mean**
High GFP	**92993**	**84.55%**	**324.14**
Low GFP	**16988**	**15.45%**	**3.64**
PF D2Z0 + G418 (40ug/mL) g=0.061			
Subpop.	**# of events**	**Percentage**	**Geometric mean**
High GFP	**38674**	**35.15%**	**290.11**
Mid GFP	**23931**	**21.75%**	**30.46**
Low GFP	**48024**	**43.64%**	**3.34**

Figure S8. Effect of slow growth rate due to ethanol and Cisplatin on ancestral PF distributions in D2Z0 at day 4. (A) Gene expression distributions. (B) Histogram statistics.

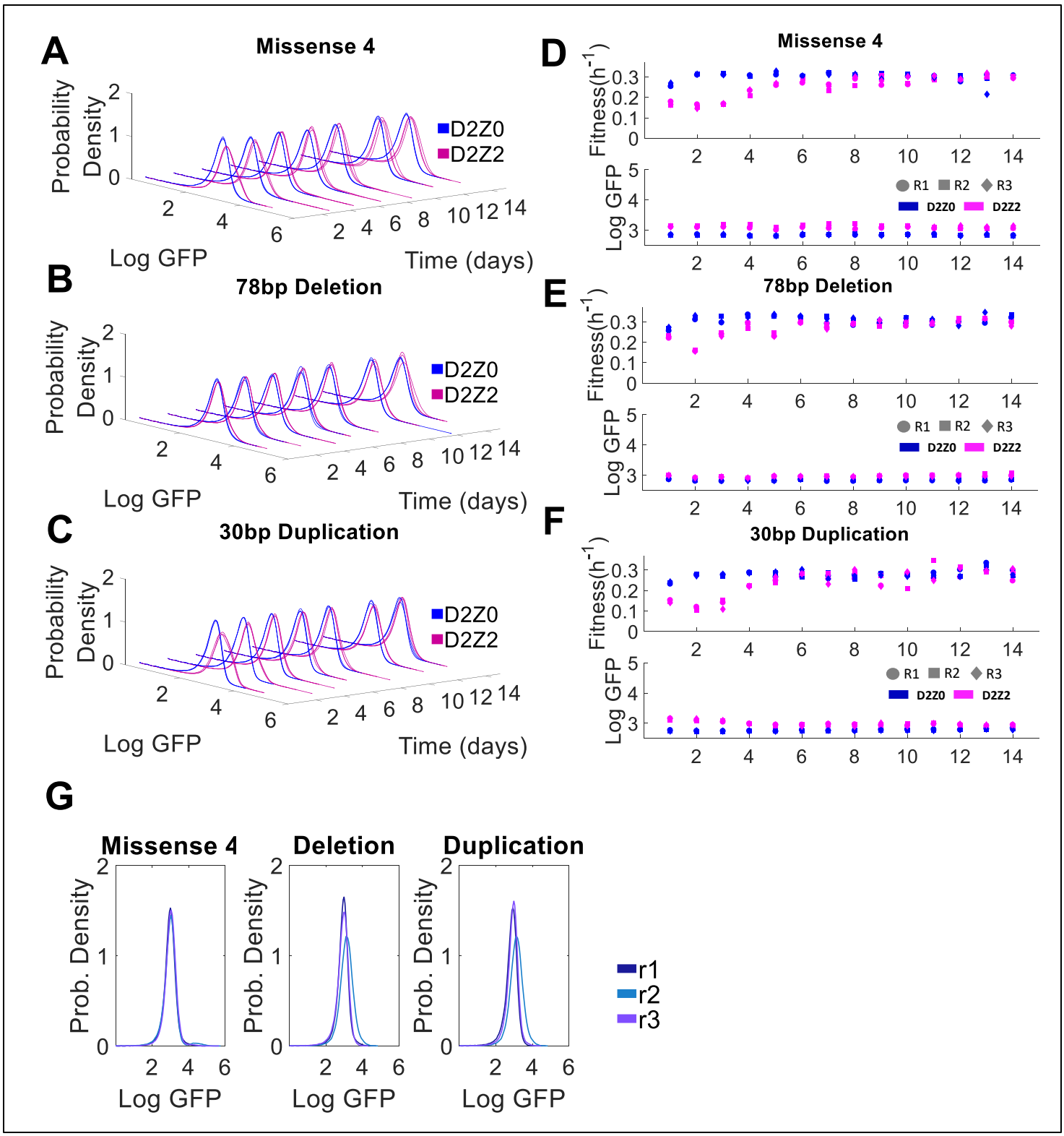

Figure S9. Evolutionary dynamics of nonfunctional mutants Missense 4, Deletion and Duplication that never regain rtTA function.

(A-C) Histograms of *yEGFP::zeoR* expression of 3 replicates of Missense 4, Deletion and Duplication mutants, respectively, in D2Z0 (blue) and D2Z2 (magenta) over the course of 14 days. These mutants do never exhibit any bimodality while evolving in D2Z2, but they develop a slightly higher basal yEGFP::zeoR mean in D2Z2 compared to the mean expression in D2Z0.
(D-F) Fitness (Left) and mean *yEGFP::zeoR* expression (Right) plots for Missense 4, Deletion and Duplication mutants, respectively, computed for each day during the experiment. Early in the experiment, we observe a drop in fitness of D2Z2 cultures compared to D2Z0 cultures. Cells cultured in D2Z2 recover within ~4 days and reach a fitness level comparable to the D2Z0 cultures. Additionally, D2Z2 cultures maintain a higher GFP expression mean compared to D2Z0 cultures for all presented mutants.
(G) Gene expression histograms of evolved population replicates hyperinduced in D6Z0 after the end of experimental evolution.

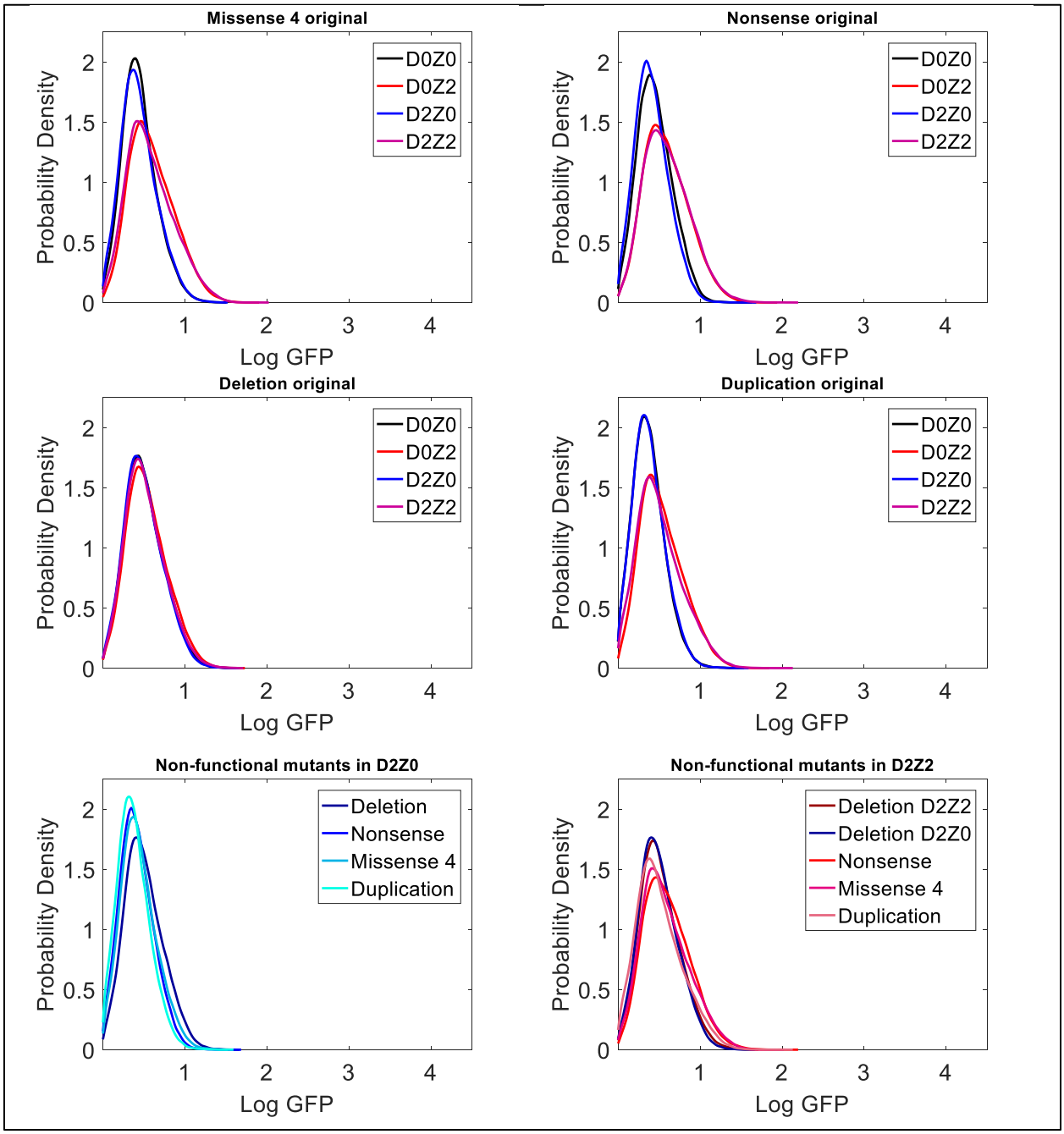

Figure S10. Phenotyping of original non-functional mutants. As opposed to the rest of non-functional mutants, plots show that the Deletion mutant does not undergo an upward shift in expression in the presence of Zeocin, indicating that it initially had yEGFP::ZeoR expression levels sufficient for cell survival in the presence of antibiotic.

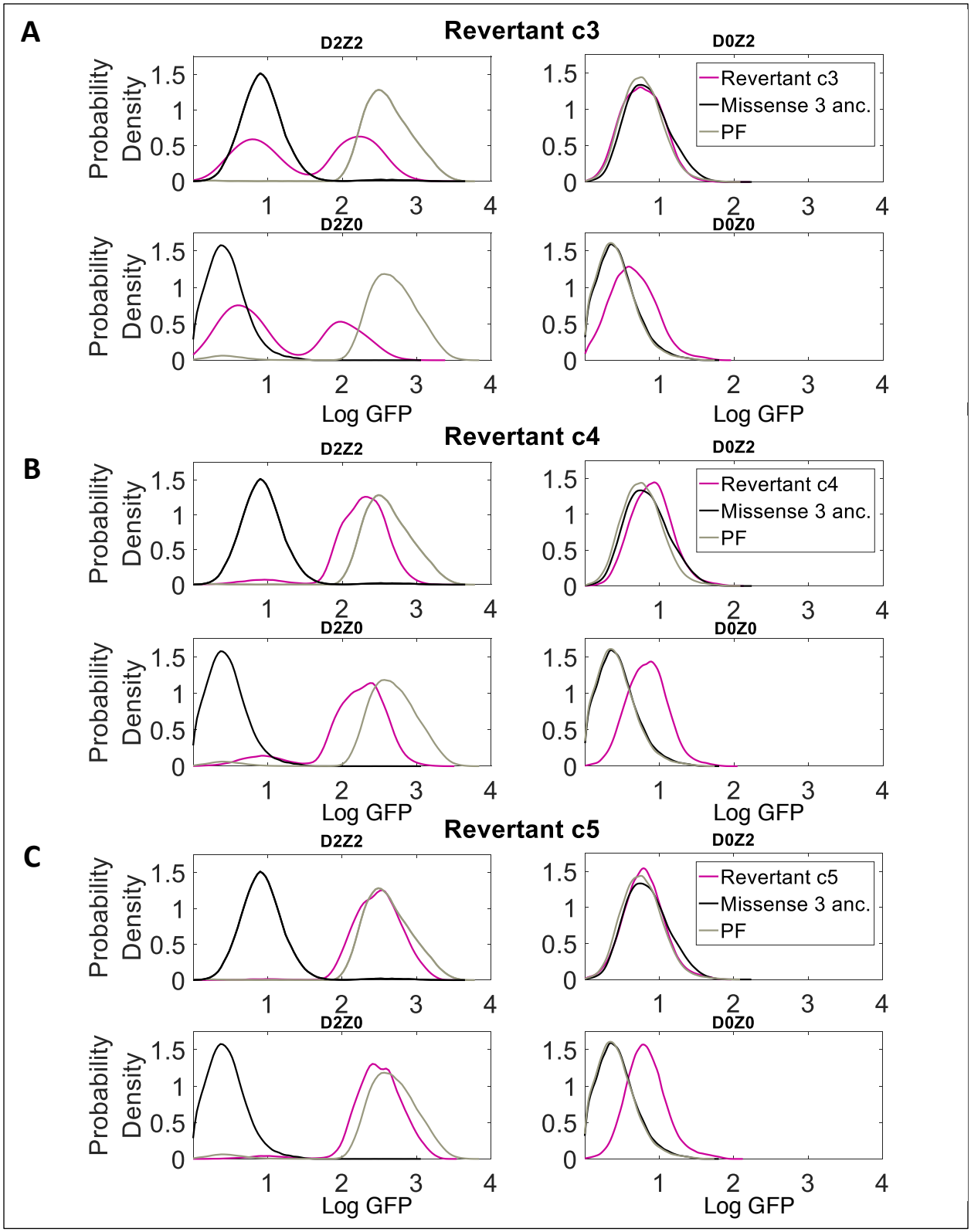

Figure S11. Gene expression distributions of three individual clones from revertant Missense 3 replicate r1 in D0Z0, D2Z0, D2Z2 and D0Z2 at day 4.

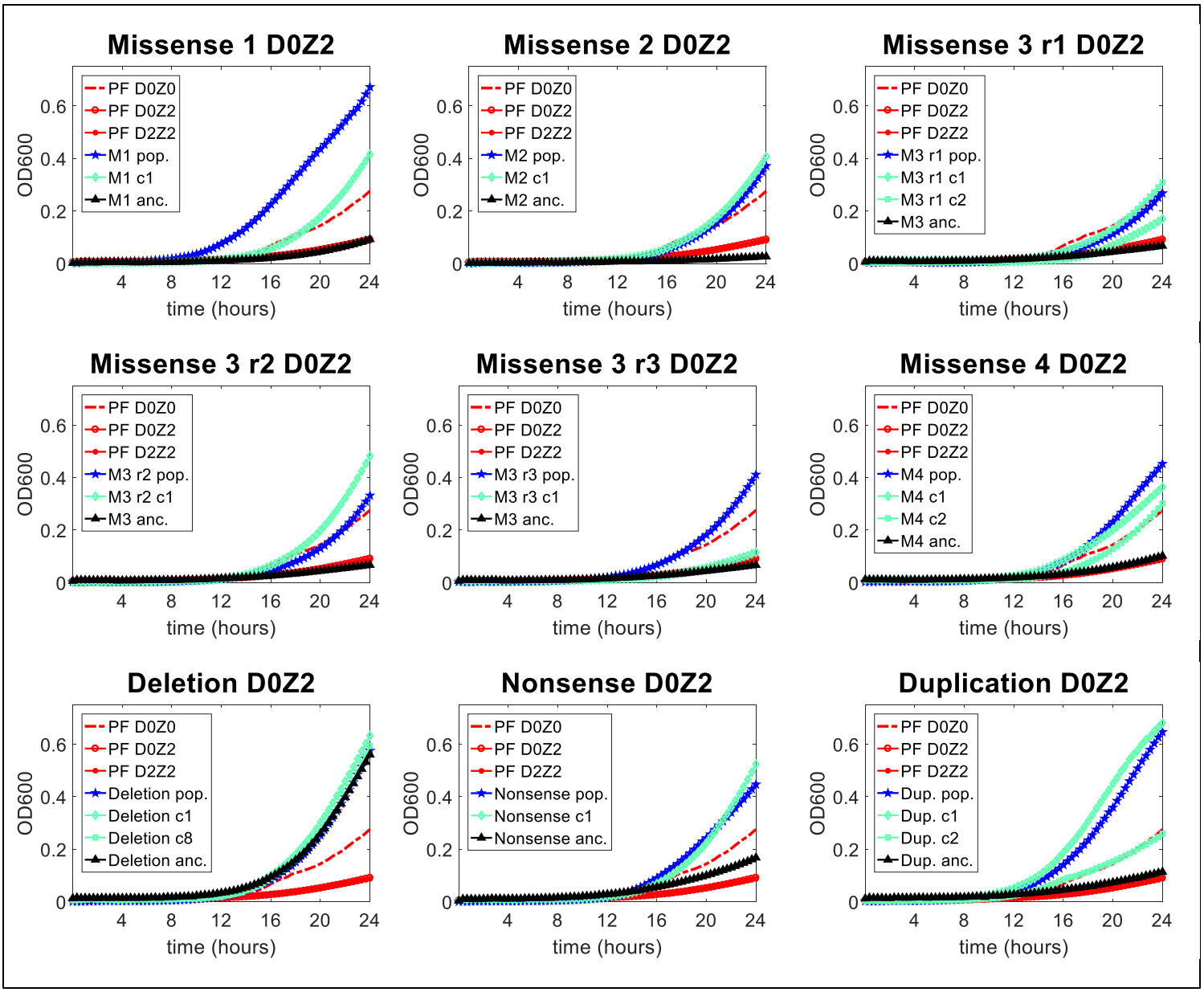

Figure S12. Growth curves of original (ancestral) mutant populations and evolved mutant population and isolated clones. Sequenced replicate 3 of all evolved mutants is represented except for Missense 3 where replicates 1, 2 and 3 are represented.

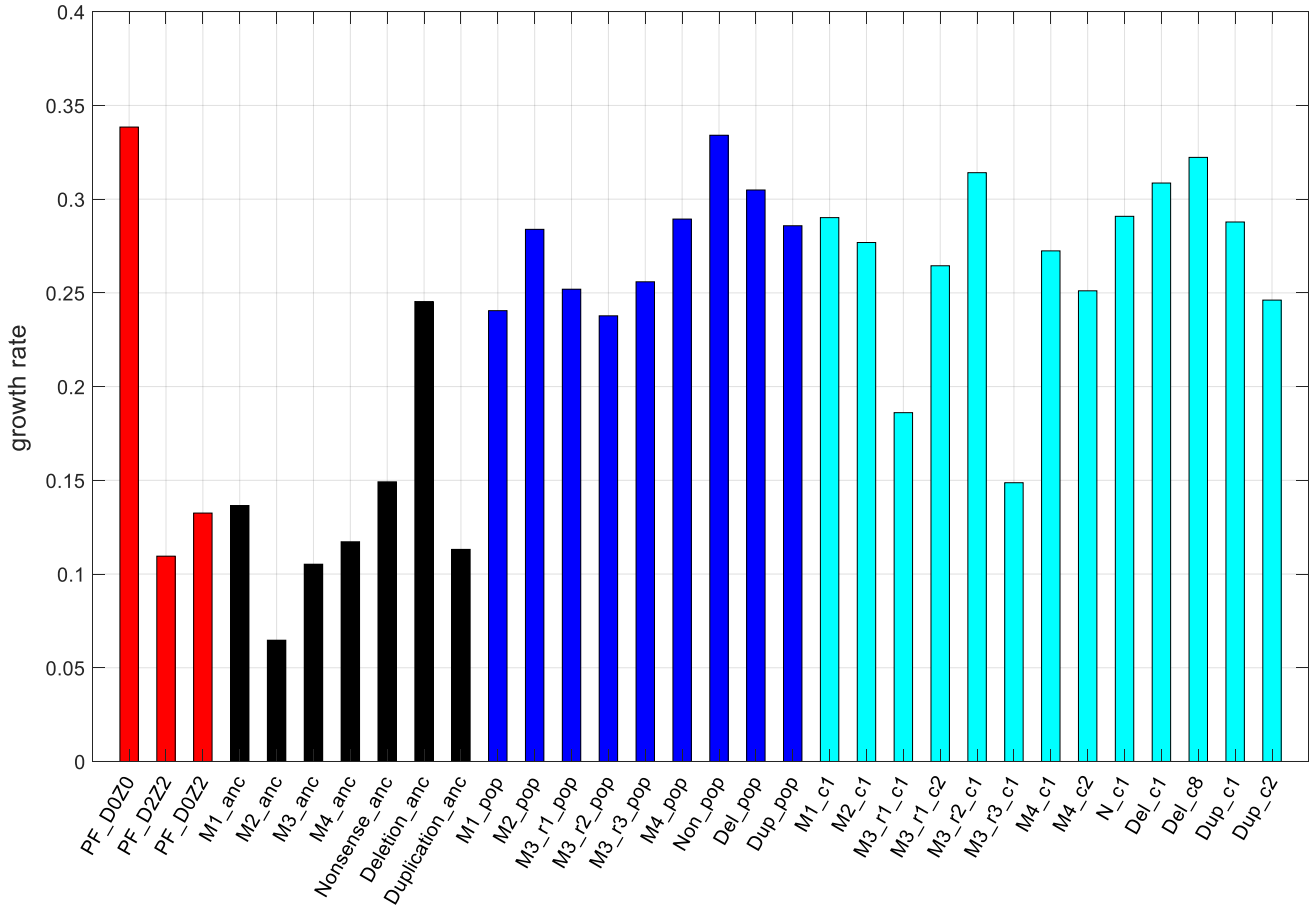

Figure S13. Exponential growth rates of original (ancestral PF) mutant populations and evolved mutant population and isolated clones estimated from growth curves in Figure S12. Sequenced replicate 3 of all evolved mutants is plotted except for Missense 3, for which replicates 1, 2 and 3 are plotted.

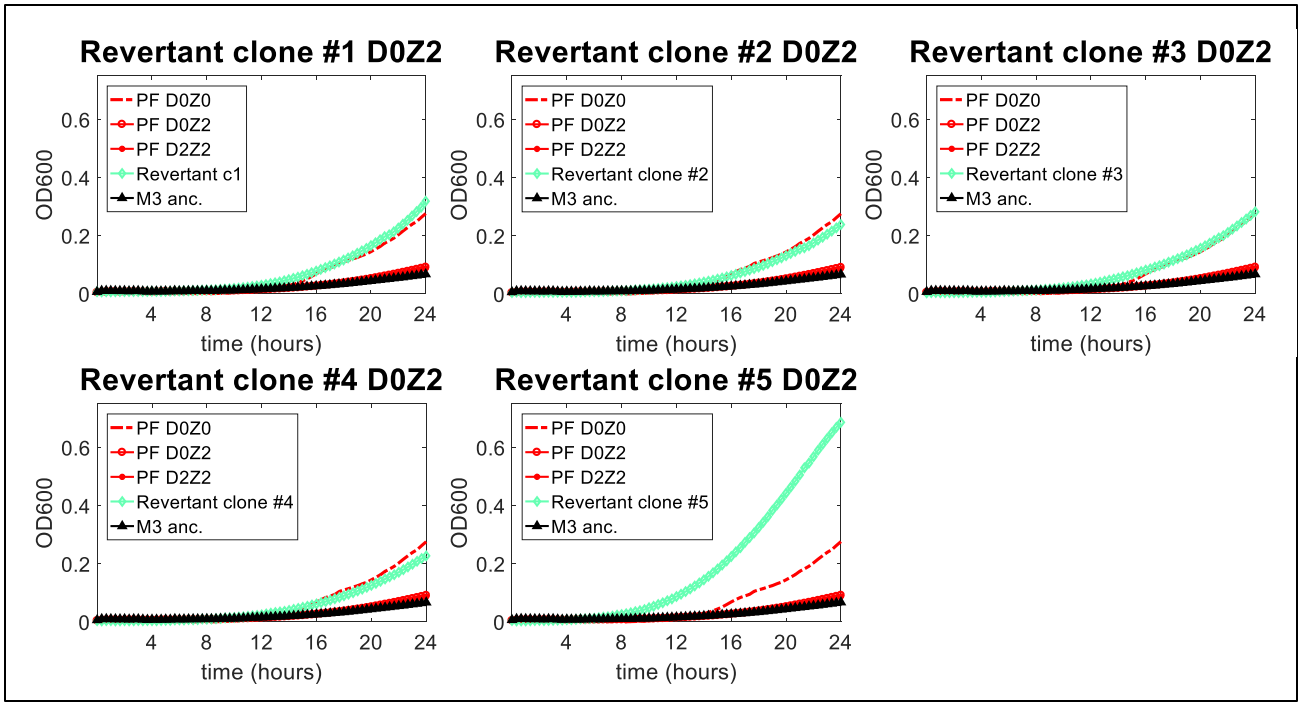

Figure S14. Growth curves of Revertant Missense 3 strains in D0Z2

4. Mathematical modeling

The goal of mathematical modeling is to qualitatively understand: (i) Wild-type PF gene circuit dynamics, e.g., why does it have two gene expression peaks above a threshold inducer concentration, and why does the position of the high peak stay relatively constant at high induction?; (ii) How did the wild-type PF gene circuit brake down in D2Z0, giving rise to quasifunctional, nonfunctional and dysfunctional mutants?; (iii) How quasifunctional and dysfunctional mutants regained high expression transiently in D2Z2, without any intra-circuit mutations, despite the rarity or complete absence of high expressors in D2Z0; (iv) How the quasifunctional and some but not all dysfunctional mutants evolved to lose high expression without intra-circuit coding sequence mutations, as described in the main text. The model is not intended to match experimental data. Instead, it illustrates qualitatively how various topological relationships between synthesis and loss curves can give robustly rise to the wild-type PF and mutant behaviors.

3.1. Deterministic (ODE) model for the wild-type PF gene circuit

To describe the wild-type, original PF gene circuit, we consider the following set of ordinary differential equations (ODEs) from [2], according to the drawing on the right:

$$\frac{dw}{dt} = aF(x) - bwy - gw + l$$
$$\frac{dx}{dt} = bwy - gx$$
$$\frac{dy}{dt} = fC - bwy - (g+h)y$$
$$\frac{dz}{dt} = aF(x) - gz + l$$

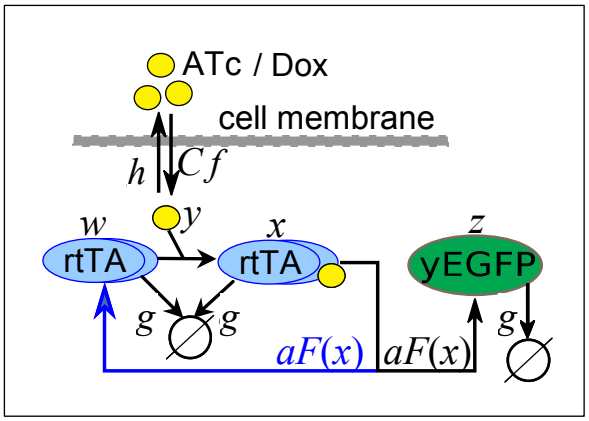

where w is inactive rtTA, x is active rtTA, y is intracellular ATc/Dox and z is yEGFP::ZeoR.

We assume that the promoter response function to active rtTA protein, x, is a Hill function:

$F(x) = \frac{x^n}{\theta^n + x^n} + l$, where θ and n are Hill parameters, and l is a promoter leakage term.

Since total rtTA and yEGFP::ZeoR obey identical equations, their levels are identical in the model: $z=x+w$. Next, we focus on inactive (inducer-free) rtTA, w, and consider the other variables to be at steady state.

In the system of ODEs that describes the PF gene circuit there is no feedback from z to any other variables. Therefore, the first three equations can be analyzed separately.

Considering the remaining two variables (other than w) at steady state we have

$$\frac{dw}{dt} = aF(x) - bwy - gw + l$$
$$0 = bwy - gx$$
$$0 = fC - bwy - (g+h)y$$

Which, after substituting w and y, yields

$$\frac{dw}{dt} = aF(x) - gx - \frac{g^2(g+h)}{b}\frac{x}{fC - gx} + l$$
$$w = \frac{gx}{by}$$
$$y = \frac{Cf - gx}{g+h}$$

Focusing only on the first equation at steady state, the solutions will give cell states:

$$\frac{dw}{dt} = a\frac{x^n}{\theta^n + x^n} - gx - \frac{g^2(g+h)}{b}\frac{x}{fC - gx} + l = 0$$

We can convert this steady-state equation into the following polynomial equation and then seek real, nonnegative solutions in Matlab:

$$bg^2x^{n+2} - g[ab + bfC + bl + g(g+h)]x^{n+1} + fbC[a+l]x^n +$$
$$+\theta^n bg^2x^2 - g[bfC + bl + g(g+h)]\theta^n x + blfC\theta^n = 0$$

Alternatively, we can also pursue a graphical solution, writing the above equation as a balance between synthesis $F_L(x)$ and loss $F_R(x)$ rates of inducer-free, inactive rtTA, w:

$$F_L(x) = a\frac{x^n}{\theta^n + x^n} + l = \frac{g}{b}\frac{bgx^2 - [bfC + g(g+h)]x}{gx - fC} = F_R(x)$$

Notice that the loss term has a *singularity* at $x=Cf/g$!

If $g(g+f)$ is much smaller than the other terms, we can simplify and have approximately:

$$F_L(x) = a\frac{x^n}{\theta^n + x^n} + l \approx gx = F_R^*(x)\,.$$

Essentially, the solutions are given by the intersection of a Hill-type, sigmoidal ***synthesis rate function*** F_L with an elbow-shaped ***loss rate function*** F_R that is a positive-sloped line $F_R^*(x)$, except when approaching the singularity at x=Cf/g from below. Any values above the singularity are non-physical.

The results are robust to parameters (modified from [2]). Changing one parameter may require other parameter changes to ensure the synthesis and loss rate curves intersect or miss each other as described below. A set of parameters closely reproducing wild-type PF dynamics (e.g., a saddle-node bifurcation at Dox=0.05 μg/mL) is the following: a=20; b=5; g=0.25; f=2; h=2.5; l=0.01; n=4; θ=0.75. In the next sections, we use slightly different parameters (as in the main text), to facilitate visualization. Parameter units can be found in [2]. The effects of the original seven mutations and then the new mutations can be modeled by parameter changes equivalent to the ones described below.

Analyzing the full equation (without making approximations, assuming n > 2), we obtain the following cases for the solutions (steady states) given by the intersections of red and blue curves. The Matlab scripts uploaded as Supporting Files produce these results.

Case 1. The line y=gx misses F_L from below. This case is discussed just for completeness; it does not correspond to PF behavior. It occurs when l is large (here, a=20; b=5; g=0.25; f=2; h=2.5; l=0.5; n=4; θ=5). The system is monostable, irrespective of Doxycycline. Only one physical solution exists, which could be low or high, given approximately by:

$$x_0 \approx \begin{cases} F_L\left(\frac{Cf}{g}\right) = \frac{a(Cf)^n}{(g\theta)^n + (Cf)^n} + l; C < a + l \\ F_L\left(\frac{a+l}{g}\right) = \frac{a(a+l)^n}{(g\theta)^n + (a+l)^n} + l; C \geq a + l \end{cases} \qquad z \approx \begin{cases} F_L\left[F_L\left(\frac{Cf}{g}\right)\right]; C < a + l \\ F_L\left[F_L\left(\frac{a+l}{g}\right)\right]; C \geq a + l \end{cases}$$

The left plot below shows the dose-responses of the biochemical species w (free rtTA), x (active rtTA), y (intracellular inducer) and z (reporter) on the left. The right plot shows the rate functions $F_R(x)$ and $F_L(x)$ from above. The thick black triangle on the first (left) plot marks the Doxycycline (C) concentration for the plot on the right. This case illustrates a capability of the generalized system to be monostable high; this is not wild-type PF behavior. Note that total rtTA, or the sum of free rtTA, w and inducer-bound rtTA, x equals yEGFP, as expected due to the identical PF promoters: $z = x+w$.

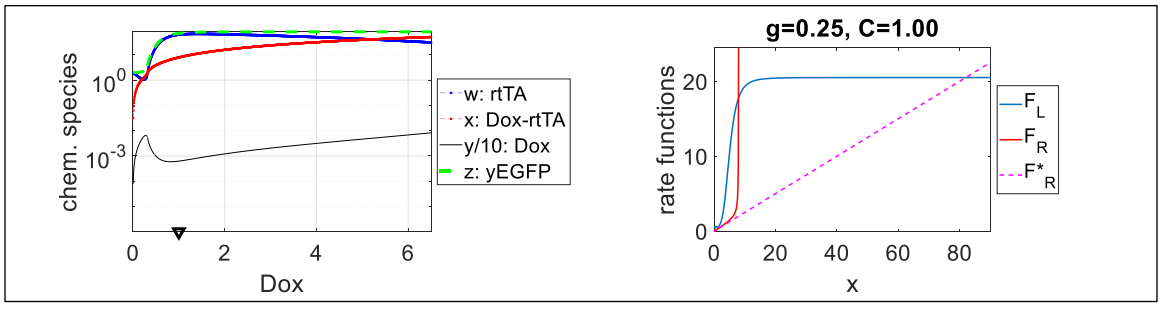

Case 2. The line $y=gx$ intersects the Hill function three times. This is the actual wild-type PF system. The number of solutions (steady states) is 1 to 3 depending on Doxycycline (C), as described below. The thick black triangle on the left plot marks the Doxycycline (C) concentration for the other plot. Denoting the three intersection points of the line $y=gx$ with the Hill-type function $F_L(x)$ by x_1, x_2, and x_3, respectively, the following subcases exist.

Subcase 2A. At low Doxycycline concentrations, the system is monostable low (one intersection). This is the PF system at low induction, below the bimodality threshold, as shown below.

$$x \approx \begin{cases} \dfrac{Cf}{g}, \text{if } \dfrac{Cf}{g} \le x_1 \\ x_1, \text{if } x_1 < \dfrac{Cf}{g} \le x_2 \end{cases} \qquad z \approx \begin{cases} \dfrac{a}{g}F_L\left(\dfrac{Cf}{g}\right)+\dfrac{l}{g}, \text{if } \dfrac{Cf}{g} \le x_1 \\ \dfrac{a}{g}F_L\left(x_1\right)+\dfrac{l}{g}, \text{if } x_1 < \dfrac{Cf}{g} \le x_2 \end{cases}$$

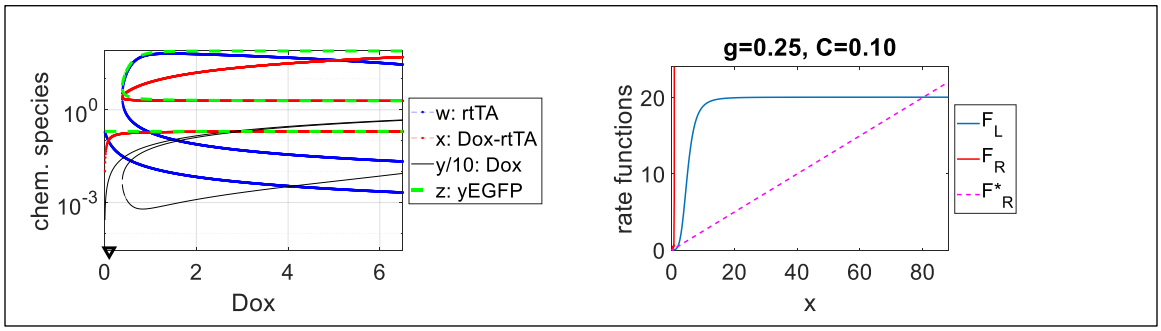

Subcase 2B. At medium to high Doxycycline concentrations, the system is bistable (three intersections). This is the PF system above the bimodality threshold. The system seems to remain bimodal for arbitrarily high Doxycycline concentrations.

$$x \approx \begin{cases} x_1, \text{if } x_1 < \dfrac{Cf}{g} \le x_2 \\ x_1, x_2, F_L\left(\dfrac{Cf}{g}\right) \text{if } x_2 < \dfrac{Cf}{g} \le x_3 \\ x_1, x_2, x_3 \approx F_L\left(\dfrac{a+l}{g}\right), \text{if } x_3 < \dfrac{Cf}{g} \end{cases} \qquad z \approx \begin{cases} \dfrac{a}{g}F\left(x_1\right), \text{if } x_1 < \dfrac{Cf}{g} \le x_2 \\ \dfrac{F_L\left[F_L\left(x_1\right)\right]}{g}, \dfrac{F_L\left[F_L\left(x_2\right)\right]}{g}, \dfrac{1}{g}F_L\left[F_L\left(\dfrac{Cf}{g}\right)\right] \text{if } x_2 < \dfrac{Cf}{g} \le x_3 \\ \dfrac{F_L\left[F_L\left(x_1\right)\right]}{g}, \dfrac{F_L\left[F_L\left(x_2\right)\right]}{g}, \dfrac{1}{g}F_L\left[F_L\left(\dfrac{a+l}{g}\right)\right], \text{if } x_3 < \dfrac{Cf}{g} \end{cases}$$

Here, to roughly capture standard PF behavior we used a=20; b=5; g=0.25; f=2; h=2.5; l=0.05; n=4; and θ=5. The behavior is shown on the plots below.

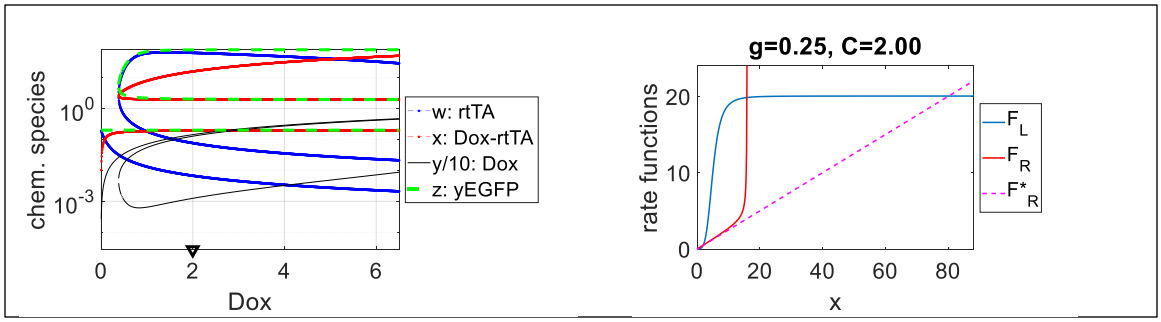

The system undergoes a saddle-node bifurcation at $Cf = gx_2$, where a new stable and an unstable node emerge. The system is bistable for any $Cf > gx_2$, thus two peaks exist even at very high Dox. The saddle-node bifurcation occurs as the loss rate function $F_R(x)$ first touches, then crosses the Hill-type synthesis rate function $F_L(x)$ from above.

Case 3. The line $y=gx$ misses the Hill function from above. This occurs when a is small, and g is large, for example. This is not standard wild-type PF behavior, it is listed here only for completeness. The system is monostable low, irrespective of Doxycycline concentration. Only one low-expressing physical solution exists, given approximately by

$$x_0 \approx \frac{l}{g} \Rightarrow z \approx \frac{1}{g} F_L\left(\frac{l}{g}\right) = \frac{a}{g}\frac{l^n}{(g\theta)^n + l^n} + \frac{l}{g}.$$

To obtain this behavior, we had: a=20; b=5; g=0.5; f=2; h=2.5; l=0.05; n=4; θ=25.

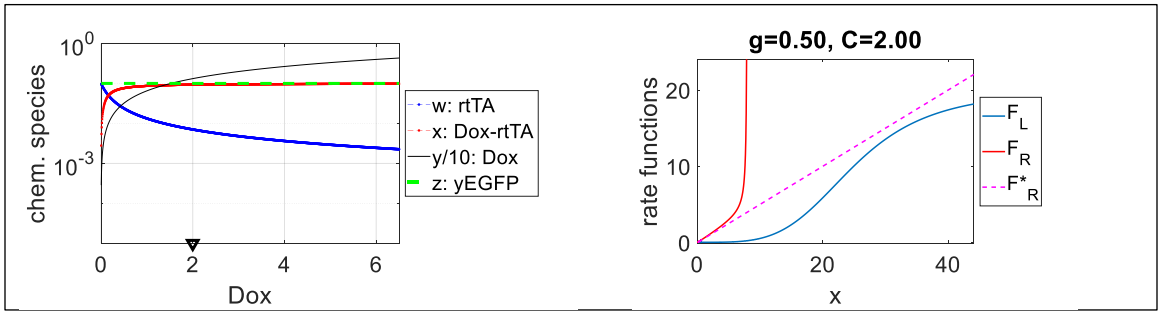

3.2. Mathematical model for the nonfunctional PF mutants

Next, we ask how the PF gene circuit can be broken in nonfunctional mutants. These mutants are monostable low, regardless of Doxycycline.

One way, of course, is to completely defunctionalize rtTA, for example by flattening the Hill (sigmoidal) synthesis rate function. This means that the promoters do not respond to rtTA, as for the Deletion and Duplication mutants. These mutants cannot become bistable under any curcumstances.

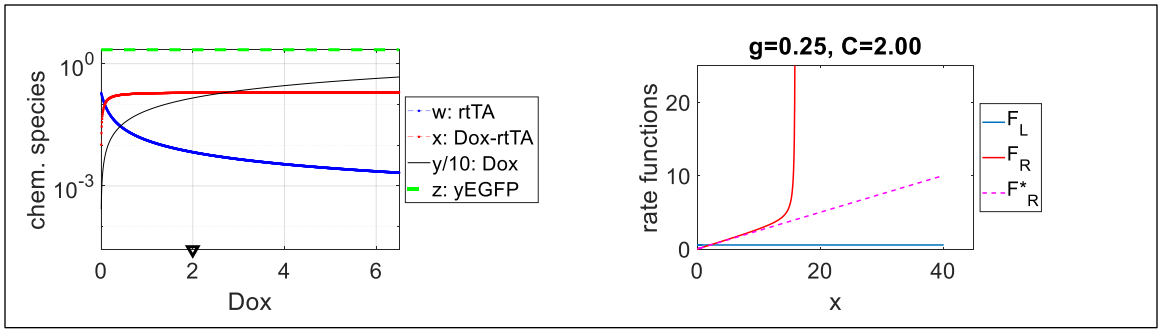

The parameters used here were: a=1; b=5; g=0.25; f=2; h=2.5; l=0.05; n=0; θ=5.

3.3. Mathematical model for the quasifunctional PF mutants

Next, we seek to explain the properties and behavior of "quasifunctional" mutants that generate a high peak due to hyperinduction with Doxycycline. One way to obtain such "quasifunctional" mutants is by increasing the Hill threshold θ compared to the original PF – for example, from 5 to 25. This can certainly happen in Missense mutants if they alter the protein's binding properties to DNA. Now the magenta line $y=gx$ will still intersect the Hill function 3 times. However, due to the singularity, in D2Z0 there is only a single intersection of the Hill function with the red elbow curve $F_R(x)$, hence the quasi-monostable low behavior in D2Z0. Note that the tiny experimentally observed high-expression peak can arise if the $F_R(x)$ and $F_L(x)$ curves barely intersect or even if they just approach each other if noise enables cells to access the high expression state.

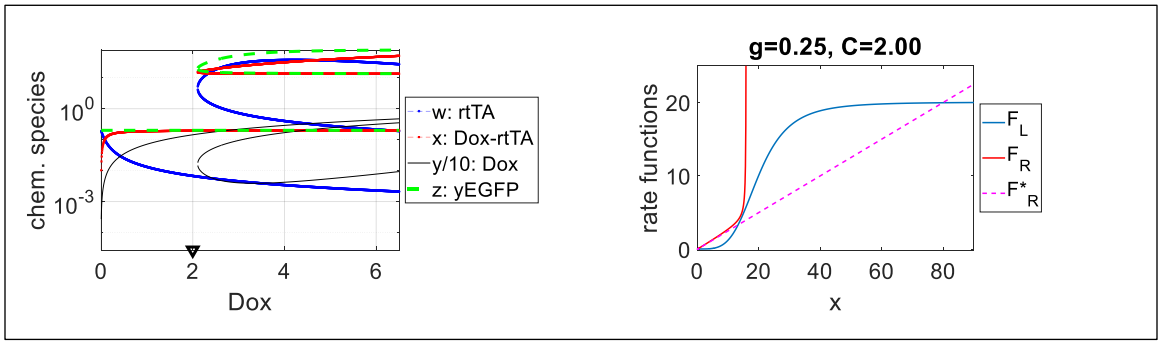

The quasifunctional parameter set is: a=20; b=5; g=0.25; f=2; h=2.5; l=0.05; n=4; and θ=25.

Below we see how bistability is recovered by hyperinduction (Dox=6μg/mL, D6Z0), which shifts the red elbow curve's singularity rightward, allowing the red curve to intersect the blue curve 3 times.

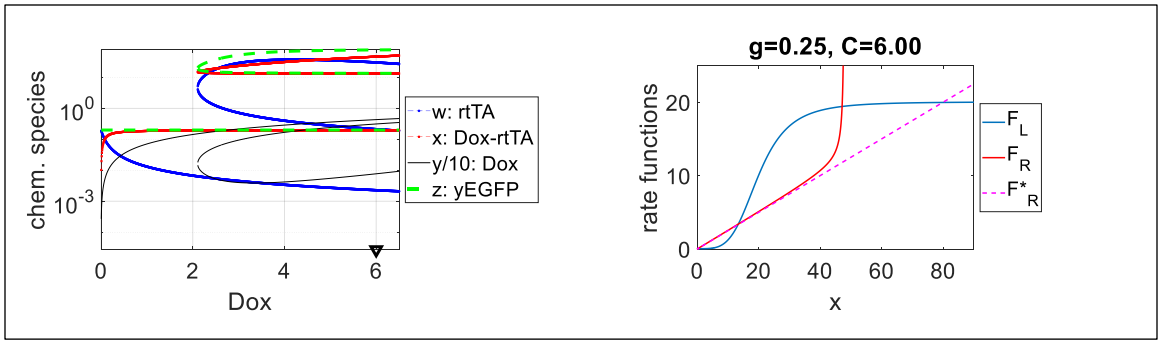

Besides hyperinduction, slow growth can also cause bistability or move the cells deeper into the bistable regime. The following plots illustrate the effect of slow growth rate (due to ethanol, Zeocin, or other factors) on the dynamics. The plots indicate that slow growth rate can convert a quasifunctional, otherwise quasi-monostable system into a bistable system, enabling high expression.

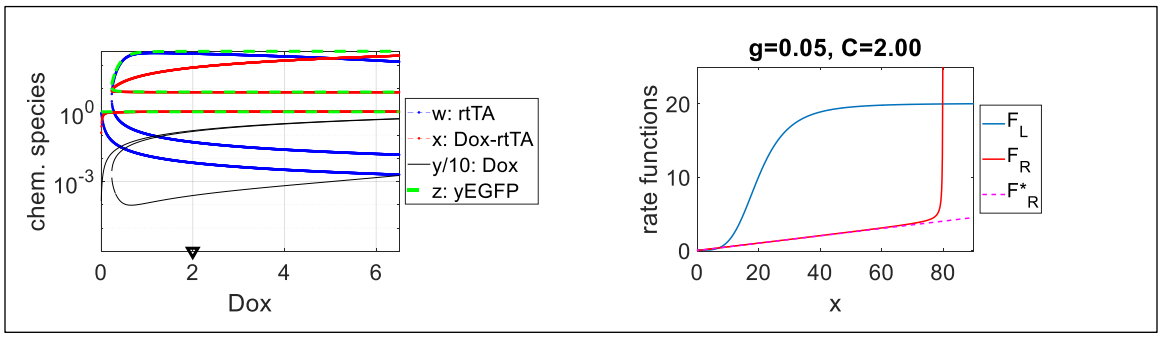

These plots imply that ethanol, Zeocin, Cisplatin or other stressors can enrich "quasifunctional" mutants in high expressors compared to pure D2Z0. So, the emergence of the high peak is due to a dynamic shift, besides phenotypic selection.

Why does the high peak diminish without any intra-circuit mutations for "quasifunctional" mutants? It is again due to a growth-related reverse dynamic shift. The bistable populations still have a low peak initially, which is hit by the drug. If any cells acquire an extra-circuit mutation that stops Zeocin from harming those low-expressor cells, their growth will accelerate, returning the whole population to the quasi-monostable low state, but now in D2Z2, as opposed to D2Z0. See the plots above.

3.4. Mathematical model for the dysfunctional PF mutant

Finally, we seek to explain the properties and behaviors of the dysfunctional mutant Missense 3. This mutant is not hyperinducible, but still develops bistability due to slow growth. One way for this to happen is if the Hill-type sigmoidal synthesis rate function shrinks (e.g., its highest level shifts down, closer to the basal level) until the magenta and red lines miss it from above, so Missense 3 will be unimodal in D2Z0 and will not respond to any hyperinduction with Doxycycline. The parameters are: a=2; b=5; g=0.25; f=2; h=2.5; l=0.05; n=4; θ=5.

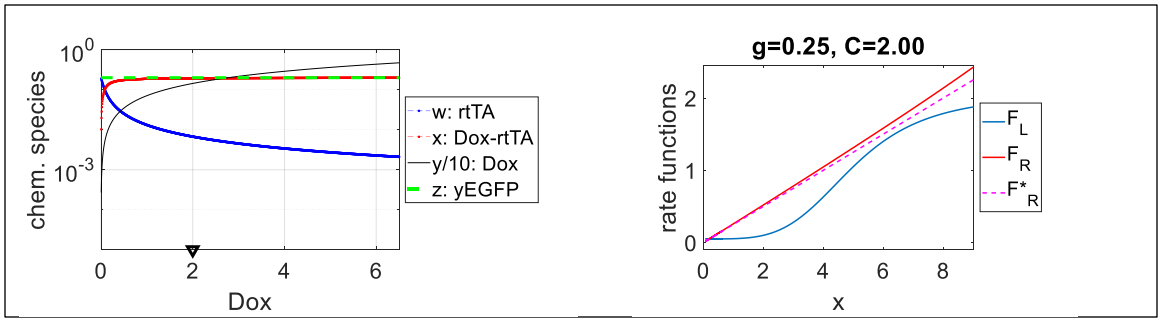

When growth decelerates due to some stressor, the red and magenta lines become less steep and can intersect the blue line 3 times, as shown below. This implies that slow growth, jointly with selection can give rise to a high expressor population, as shown below. The parameters are: a=2; b=5; g=0.05; f=2; h=2.5; l=0.5; n=4; θ=5.

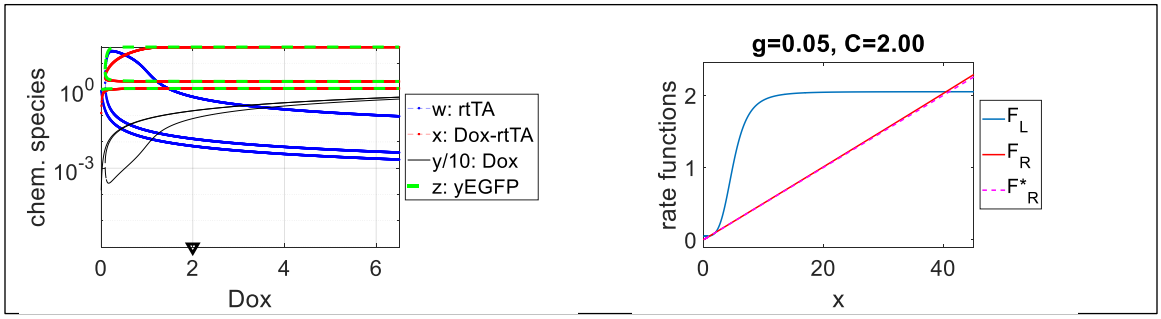

If subsequent drug-resistance mutations only speed up growth without lifting the $F_L(x)$ curve sufficiently, then the system should switch back to monostability. Indeed, we see that tendency in the population. However, some clones do fully revert and maintain bistability. How is that possible? If extra-circuit, genomic mutations increase gene expression in general (i.e., they shift the entire $F_L(x)$ function upward) then this ensures 3 intersections that will be robust to growth acceleration. The following plots illustrate the effects of a 10-fold promoter leakage increase, from 0.05 to 0.5 while growth stays normal. The parameters are: a=2; b=5; g=0.25; f=2; h=2.5; l=0.05; n=4; θ=5.

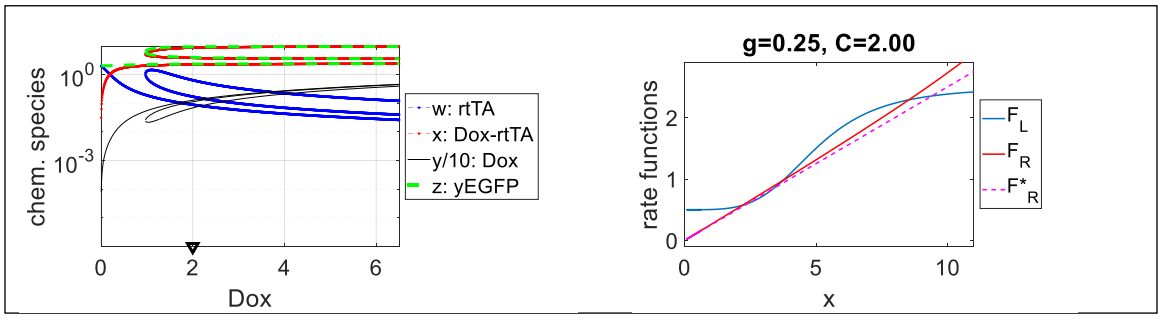

This means that the ancestral dysfunctional mutant cannot have high expression, no matter how high the concentration of inducer. Yet, the dysfunctional system is not fully broken; it still has a bistable regime and it can still achieve bistability. The new mutants can maintain high expression if they can elevate the sigmoidal synthesis curve

sufficiently. Notice that the steady states in the revertant are closer than in the ancestor, corresponding to the gene expression peaks approaching each other, as observed.

Another case. For the sake of completeness, we also mention another possibility for a mutant to be dysfunctional, that is, uninducible by hyper-induction, but still inducible by slow growth. This can happen if the Hill threshold parameter θ increases by a large amount, causing line $y=gx$ to always miss the $F_L(x)$ rate curve from above, regardless of Doxycycline. We could achieve this by increasing θ from 5 to 50, which shifts the $F_L(x)$ function rightward (compare the following plots with the wild-type PF plots above). The altered parameter set is: a=20; b=5; g=0.25; f=2; h=2.5; l=0.05; n=4; and θ=50.

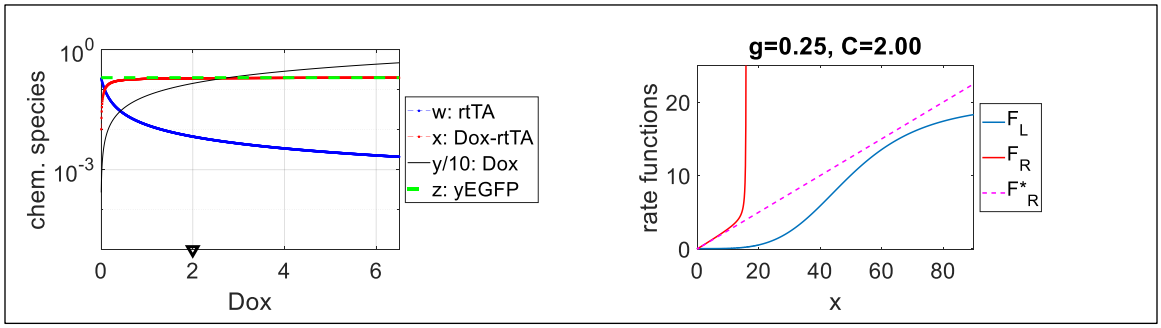

Just like the other dysfunctional mutants, such mutants could still exhibit high expression, despite being uninducible at any Doxycycline level. Slow growth, due to ethanol or Zeocin added to D2Z0 will tilt the red and magenta lines downwards, enabling them to intersect the blue $F_L(x)$ Hill-type synthesis rate function, as illustrated in the following plots. When growth speeds up again, but without the mutations affecting $F_L(x)$, bistability should be lost again. The parameter set here was a=20; b=5; g=0.05; f=2; h=2.5; l=0.05; n=4; and θ=50.

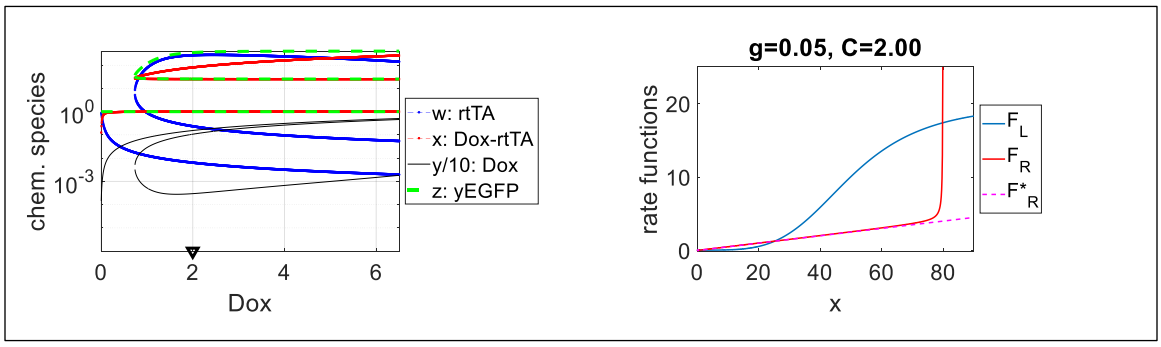

The only way to regain bistability for such mutants would be for the mutations to lower the $F_L(x)$ threshold by a large amount. This would require rtTA or PF promoter mutations. We do not think that the observed mutations are consistent with this behavior, so we consider it irrelevant to this evolution experiment.

References

1. González, C., et al., *Stress-response balance drives the evolution of a network module and its host genome.* Molecular Systems Biology, 2015. **11**(8).
2. Nevozhay, D., et al., *Mapping the Environmental Fitness Landscape of a Synthetic Gene Circuit.* PLoS Computational Biology, 2012. **8**(4): p. e1002480.
3. Deatherage, D.E. and J.E. Barrick, *Identification of mutations in laboratory-evolved microbes from next-generation sequencing data using breseq.* Methods in molecular biology (Clifton, N.J.), 2014. **1151**: p. 165-188.